Polymer 54 (2013) 4059–4077

Contents lists available at SciVerse ScienceDirect

Polymer

journal homepage: www.elsevier.com/locate/polymer

Feature article

Confinement effects on polymer crystallization: From droplets to alumina nanopores

Rose Mary Michell [a], Iwona Blaszczyk-Lezak [b], Carmen Mijangos [b], Alejandro J. Müller [a,*]

[a] Grupo de Polímeros USB, Departamento de Ciencia de los Materiales, Universidad Simón Bolívar, Apartado 89000, Caracas 1080-A, Venezuela
[b] Instituto de Ciencia y Tecnología de Polímeros, CSIC, Juan de la Cierva, 3, 28006 Madrid, Spain

ARTICLE INFO

Article history:
Received 24 March 2013
Received in revised form
9 May 2013
Accepted 10 May 2013
Available online 21 May 2013

Keywords:
Confinement
Surface nucleation
First order crystallization kinetics

ABSTRACT

We review previous works on polymer confined crystallization employing strategies that allow confinement to go from the micron to the nanometer scale: droplets, blends, block copolymers and infiltration into alumina nanopores. We also present novel results, reporting homogeneous nucleation and first order crystallization kinetics, for the first time, in a homopolymer and a diblock copolymer infiltrated within alumina nanopores. Confinement can produce fractionated crystallization or exclusive crystallization at much higher supercoolings as compared to bulk polymers, as the degree of confinement increases. For highly confined heterogeneity free micro or nano-domains, the overall crystallization kinetics is dominated by nucleation and therefore becomes first order. The nucleation mechanism changes from heterogeneous nucleation for the bulk polymer to surface or homogeneous nucleation for ensembles of confined and isolated heterogeneity free micro or nanodomains. Surface nucleation is more commonly found than homogenous nucleation, although this fact is not frequently recognized in the literature.

1. Introduction

Polymer crystallization is still far from being completely understood. Hence, it is the subject of many fundamental and practical investigations since crystallinity degree and superstructural morphology greatly influence thermal and mechanical properties that in turn determine practical applications [1–9].

One intriguing aspect, that has become more relevant with the advent of nanotechnology, is crystallization under confinement. A confined polymer system can be prepared by dividing a bulk polymer into a series of domains of reduced dimensions which are independent from one another (droplets, cylinders, lamellae, etc.). Many confined systems can span a large size range from the micron to the nanometer scale (depending on sample preparation or composition). We will refer to these isolated crystallizable domains, as microdomains (MDs), even though in many cases their size can reach nanoscopic dimensions. These polymeric MDs can experience confinement in one, two or three dimensions and it is possible to find them in droplet dispersions, blends, block copolymers, nanolayers and polymers infiltrated within inorganic templates [10–17].

When the number of MDs is of the same order of magnitude or higher than the number of active heterogeneities present in a bulk polymer, the nucleation and crystallization of the polymer can experience dramatic changes. In confined polymers, one of two situations arises during solidification from the melt:

(a) The crystallization occurs in a single crystallization event but at much lower temperatures than the usual crystallization temperature (T_c) of the bulk polymer. This is usually encountered in a system characterized by heterogeneity free MDs (or clean MDs), when the number of MDs is several orders of magnitude higher than the number of heterogeneities present in the bulk polymer.
(b) The crystallization is split into several steps well spaced in temperature. This situation occurs when the number of active heterogeneities is of the same order of magnitude than the number of MDs. Since the crystallization occurs in several steps, it is often referred to as “fractionated crystallization”, and it is usually the result of having a mixture of heterogeneity free MDs with substantial populations of MDs that contain different types of heterogeneities (i.e., heterogeneities that can be activated at different supercoolings).

In the case of heterogeneity free or clean MDs, the nucleation typically changes from a heterogeneous nucleation (present in the bulk polymer) to either homogeneous nucleation or surface nucleation of the MDs (i.e., initiated at the surface of the MDs or at the interface between the crystallizable MDs and the matrix surrounding them). Surface nucleation can be frequently encountered

* Corresponding author.
E-mail address: amuller@usb.ve (A.J. Müller).

0032-3861
http://dx.doi.org/10.1016/j.polymer.2013.05.029

(although not often recognized in the literature), since it requires a lower free energy as compared with homogeneous nucleation.

In this paper, we will discuss in detail the conditions that are required to encounter homogeneous or surface nucleation during the crystallization of confined MDs. The detection of a lower T_c value than that exhibited by the bulk polymer is not the only requisite for homogeneous nucleation, as often claimed in the literature. The order of the isothermal crystallization kinetics, the difference between T_c and T_g, and the volume of the MDs should also be taken into account, as discussed in detail below. The consequences of confinement on the nucleation, crystallization and degree of crystallinity will be discussed.

After a brief literature review that also features our previous work on polymer blends and block copolymers, we will concentrate on discussing recent works on the infiltration of polymers within alumina nanoporous templates and we will report our latest unpublished results on this salient topic in recent literature.

2. Crystallization of droplet dispersions

It was as early as 1880 when Van Riemsdyk [18] reported that small gold droplets crystallized at much larger supercoolings than bulk gold. Later (between 1948 and 1969), many researchers performed careful experimental studies on droplet dispersions (usually in the micron range) of water, metals, alkanes and polymers [19–28]. All these studies reported that the crystallization of droplets occurred at much greater supercoolings than in the bulk material. The explanation offered was a change from heterogeneous nucleation in the bulk polymer to a different kind of nucleation in heterogeneity free droplets. The nucleation could occur by the generation of homogeneous nuclei in the bulk of the droplets or by surface nucleation. In several of these works, the authors pointed out that surface nucleation required a lower free energy and therefore could dominate the crystallization of clean droplets, rather than the more energetically costly homogeneous nucleation that should occur within the volume of the droplet by spontaneous aggregation of the molecules.

Dalnoki-Veress and coworkers [29–35] revisited recently these classic droplet experiments by employing a new and ingenious method to produce clean droplet dispersions. They focused their attention on the crystallization of droplet dispersions of poly(-ethylene oxide), PEO, and polyethylene, PE. They prepared thin films by spin coating PEO or PE onto immiscible substrates (like polystyrene films), and in a second step the sample was annealed to induce dewetting. The droplets thus produced were studied by polarized light optical microscopy (PLOM), atomic force microscopy (AFM) and elipsometry.

The crystallization of the droplets was followed by direct observation in the optical microscope. The sample was slowly crystallized; the time and the number of droplets that solidified were recorded. Two different kinds of behavior were observed. At higher temperatures, the heterogeneously nucleated droplets crystallized, while at a lower crystallization temperature the clean droplets (e.g., homogeneously or surface nucleated droplets) crystallized. An important advantage of these experiments is the possibility to verify the nature of the nucleation process.

Employing a correlation plot for successive melting and cooling experiments, it is possible to deduce if the nucleation of the droplets occurs in droplets that contain heterogeneities or in clean droplets (where probably homogeneous nucleation can take place within the volume of the droplet) [29–35].

Fig. 1 shows typical results, where the droplets crystallization temperatures of two consecutive experiments are plotted versus one another. In the case of heterogeneously nucleated droplets, the temperature of the crystallization should always be the same for each droplet. Each heterogeneity has a particular energy barrier, in consequence, it has a particular crystallization temperature. Therefore, there is a good correlation around the line where $T_{c1} = T_{c2}$ (see Fig. 1b). However, in the case of homogeneous nucleation a poor correlation was found between successive crystallization temperatures (Fig. 1a). Homogeneous nucleation depends on the nature of the polymer and on the size of the droplets. Therefore the droplets with the same size have similar crystallization temperature and the data seems to cluster around specific values (Fig. 1a).

In the case of homogeneously nucleated droplets, it is possible to establish a relationship between the crystallization temperature and the droplet volume, since the probability of nucleation depends on the volume [11,19,29].

Massa et al. [31] also found that the homogeneous nucleation process does not depends on the molecular weight or chain length. According to the results obtained on PS-*b*-PEO block copolymers, the homogeneous nucleation of the PEO block is only affected by closely neighboring chain segments and not by the entire macromolecule.

Recently, Carvalho and Dalnoki-Veress [33] studied the different types of nucleation that can occur in droplet dispersions. They studied the crystallization of PEO droplets on substrates of varying roughness (amorphous or semi-crystalline isotactic polystyrene), and in all cases they found a behavior similar to Fig. 1, where a group of droplets exhibited a correlation plot of the type shown in Fig. 1b (at low supercoolings) while a second group of droplets exhibited correlation plots similar to Fig. 1a (at high supercoolings). They concentrated in studying the crystallization of clean droplets that freeze at high supercoolings.

By performing direct visualization of droplet solidification at constant temperatures, they were able to obtain nucleation kinetics data from which a time constant (τ) can be extracted that characterizes the nucleation process [29,33]. For classic homogeneous nucleation, this time constant should scale with the radius of the droplets as: $\tau \sim R^3$, as demonstrated in Ref. [29] for PEO droplets dewetted on smooth amorphous atactic PS surfaces.

Carvalho and Dalnoki-Veress [33] obtained that the scaling of the time constant for nucleation varied depending on the roughness of the surface upon which the droplets are deposited. Scaling exponents for clean droplets corresponding to 3 (nucleation within the volume of the droplets or classic homogenous nucleation), 2 (surface nucleation) and 1 (for droplets nucleated at the contact line between the surface and the droplet, referred to as edge nucleation) were found for clean droplets. Fig. 2 shows AFM images that apparently indicate the exact location of primary nuclei in selected droplets. Additionally, the droplets which exhibited surface or edge nucleation, needed less supercooling than volume nucleated droplets.

According to the correlation plot approach (Fig. 1), all the cases examined by Carvalho and Dalnoki-Veress [33] corresponded to non-heterogeneous nucleation (which they claimed were homogenous nucleation in all cases). Nevertheless, in this paper, we will only refer to “homogenous nucleation” in the case where primary nuclei start inside the volume of clean droplets, since this is the only situation considered in classic nucleation theory as truly homogeneous nucleation (in the sense that no heterogeneity or surfaces play a role in the spontaneous aggregation of atoms or molecules to form primary nuclei within a MD). The other cases where the scaling has been found as 2 or 1 can be considered special cases of surface or edge nucleation and they occur at lower undercoolings as compared to homogeneous nucleation.

The works reviewed above indicate that the nucleation of droplet dispersions is a complicated process, where at least four types of situations can arise:

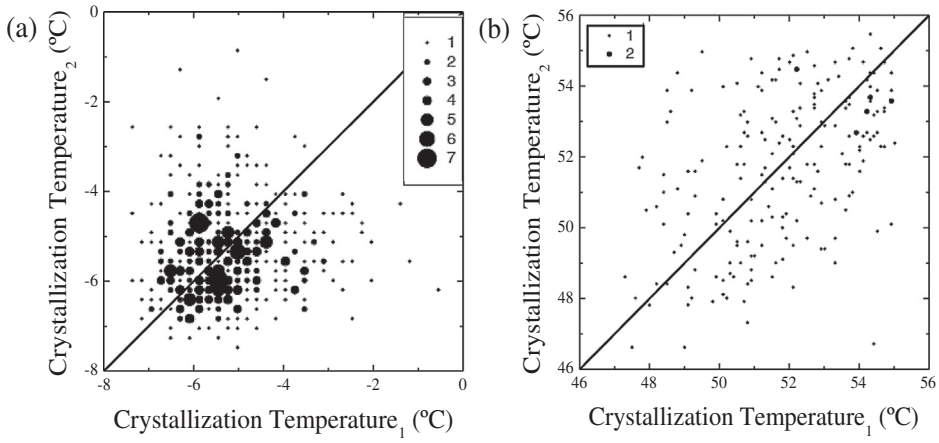

Fig. 1. Correlation plots for POE droplets: (a) homogeneous and (b) heterogeneous nucleation. The legend indicates the number of droplets which crystallize at the same temperature [35].

(1) *Heterogeneous nucleation*. Upon cooling from the melt, the first group of droplets that can crystallize are those that contain highly active heterogeneities. The nucleation occurs at low supercoolings at temperatures equivalent to those for the bulk polymer in a classic heterogeneous nucleation case. When different types of heterogeneities are present, less active heterogeneities may trigger nucleation at higher supercoolings. This case gives rise to the so called fractionated crystallization that has been observed in blends and block copolymers (see below and reviews about the phenomenon in Refs. [10,11,16,36]).

(2) *Nucleation at large supercoolings of clean droplets or MDs*. Upon further cooling, the clean droplet population can crystallize at larger supercoolings depending on their size and interfacial characteristics. As demonstrated by Carvalho and Dalnoki-Veress [33] if the droplets are in contact with an external surface, this surface can also induce nucleation. Therefore, even in clean droplets, three cases must be considered at increasing supercoolings, depending on the roughness of the surface in contact with the droplet: (a) edge nucleation, (b) surface nucleation and finally (c) classic homogeneous nucleation, at the maximum possible supercooling (taking into consideration the volume of the droplets or MDs)

Additionally, the isothermal crystallization kinetics in the case of heterogeneous nucleation is that usually encountered in semicrystalline polymers, where the Avrami index takes values of 3–4 (or even 2 in some cases). On the other hand, as explained in detail below, when the crystallization of heterogeneity free MDs is considered (usually taking place at large supercoolings), a first order crystallization kinetics (or lower) is normally obtained (i.e., an Avrami index of 1).

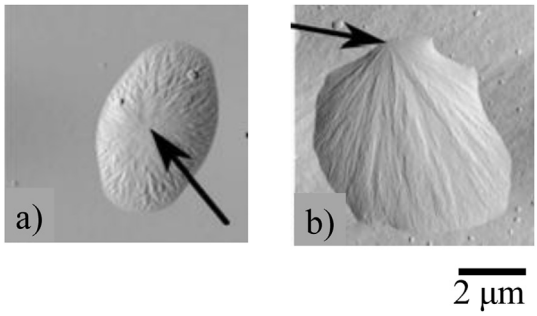

Fig. 2. AFM images of PEO droplets on different PS substrates: (a) Possible homogeneous nucleation within a droplet interior, (b) nucleation at the contact line or edge nucleation [33].

Therefore, it should be readily apparent that encountering classic homogeneous nucleation, where chains spontaneously aggregate within the volume of the MDs under consideration would not be common. The differences in supercooling needed for the different types of nucleation are a function of the energy barriers involved, and the largest energy barrier is that encountered by polymer chains to nucleate homogeneously.

Although true homogeneous nucleation has been documented for PEO droplets, there are other polymers like polyethylene (PE), where surface nucleation dominates and careful examination of the literature indicates that classic homogeneous nucleation (despite claims to the contrary, in papers where just low values of crystallization temperature have been considered instead of surface nucleation) has never been observed for the case of PE droplets, blends or block copolymers (see Refs. [11,16,34,36,37] and references there in).

Related studies of droplets crystallization have been reported for dispersions created with a wide range of techniques: dewetting [38], miniemulsion and aqueous dispersions [39–44], preparation of nanodroplets by annealing multilayer films obtained by coextrusion and nanolayers [45–54].

Kailas et al. [38] prepared dispersions of isotactic polypropylene (PP) nanodroplets, by spin coating and subsequent dewetting. They studied their in-situ crystallization by hot-stage AFM. These PP droplets are pancake like droplets since they are flattened, so their diameters are much larger than their thickness. Three types of nucleation events were found and they observed that the nucleation depended on the volume and on the thickness of the droplets in contrast to the findings of Massa et al. [31]. Kailas et al. [38] explained the difference arguing that in their work they go down to 2 nm in thickness size, while the minimum thickness employed by Massa et al. is 5 nm, and this difference in size may affect the confinement level. The authors reported three types of behavior: 1. Instantaneous nucleation and quick crystal growth in isolated nanodroplets with thickness greater or equal to 5 nm. The crystallization temperatures observed were in the range of 38 to 37 °C, and T_c had a dependence on droplet volume. 2. Nucleation and slow growth where only one nucleus was formed inside the droplets. This behavior was observed in droplets whose thickness was between 2 and 3 nm with a diameter around 700 nm. The crystallization temperature was 34.8 °C. 3. Multiple nucleation

within the droplets accompanied by slow growth. This behavior was found for thicknesses of 3.5–5 nm and a crystallization temperature of 33 °C.

Kailas et al. [38] argued that at high degrees of confinement, the thickness and volume of the droplets influence the nucleation temperatures observed and the way in which the crystalline structure growths. In droplets whose thickness is very small (lower than 5 nm), the dimensions of the critical nucleus are comparable to the thickness of the droplets. These results are explained in terms of thickness dependence and are not attributable to surface nucleation. AFM studies as a function of temperature demonstrated that during heating scans, reorganization processes occur that transformed the PP crystalline phase from the smectic to the alfa modification.

One curious observation from the results obtained by Kailas et al. [38] is the fact that the minimum crystallization temperature reported for 0.5 nm thickness PP droplets is 24 °C. This temperature presumably corresponds to the crystallization of homogeneously nucleated PP droplets. The homogeneous nucleation temperature for these extremely small nanodroplets is still 24 °C above the T_g of PP (whose T_g is approximately 0 °C). In the case of PEO and PCL nano-spheres within diblock and triblock copolymers (with a size between 10 and 20 nm), the homogeneous nucleation observed during DSC cooling scans occurs at temperatures that only differ approximately 1–5 °C from their respective T_g values [11]. Homogeneous nucleation should occur at the maximum available supercooling. It is therefore, still unknown why in PP, the homogeneous nucleation temperature can occur at such relatively high nucleation temperatures.

Other approaches to prepare droplet dispersions to study their crystallization have been reported by Montenegro and Lanfester [39], Tongcher et al. [40], Taden and Lanfester [41] (mini-emulsions) and by Ibarretxe et al. [43] (aqueous dispersions of polyolefins).

1-D spatial confinement of polymers can be obtained in thin films with a concomitant effect on their crystallization behavior. The formation of crystal nuclei will be drastically affected (especially at higher temperatures). Also, the preferential orientation of polymer crystals will also be influenced by 1-D confinement, a phenomenon that has been carefully studied [45,55–71]. The effects of film thickness can be summarized into several categories:

a. Thickness of several hundred of nanometers. In this case, predominantly edge-on lamellar crystals have been found obtained. Examples can be found for: isotactic polypropylene [56,57], multilayer coextruded iPP/polystyrene [45], polyamide 6 [58], poly(ethylene oxide) [59], poly(ethylene naphthalene) [60], poly(ethylene terephthalate) [61] and PEO in poly(vinyl chloride) blends [62].
b. "Ultrathin films" (thickness < 100 nm). In these cases, the film thickness can approach the average size of the polymer coils, this characteristic will provoke the formation of flat-on (flattened) lamellar crystals. Reported examples include: poly(vinylidene fluoride) [63], PEO [64] and poly(3-hydroxybutyrate) [66].
c. "Quasi-Two dimensional" thin films. This category encompasses those thin films where the crystallization becomes diffusion-limited, as shown by experiments using PEO [67–69], PE [70] and PET [71].

Upon decreasing film thickness, the morphological transition from edge-on to flat-on crystals has been observed in wide range of polymers [45,55–71]. It has been argued that this transition reflects the influence of the spatial confinement by the film thickness upon the formation of the crystal nuclei. A detailed discussion of thin films is beyond the scope of the present contribution.

3. Crystallization of confined components within polymer blends

The morphology of immiscible polymers blend depends on composition. When the amount of the dispersed phase is small (~20%) the formation of droplets of a micrometric size is commonly reported [72]. In these cases a confined environment is obtained. If the dispersed component can crystallize, it may exhibit fractionated crystallization. This term was coined by Frensch et al. [10] to describe the multiple crystallization exotherms that can be observed when an ensemble of MDs (e.g., the dispersed micro-droplets within a matrix in an immiscible polymer blend) is cooled from the melt in a DSC, as opposed to single crystallization exotherm exhibited by bulk homopolymers.

One important condition for fractionated crystallization to occur is that the number of MDs should be at least of the same order of magnitude or higher than the number of active heterogeneities in the bulk polymer. When a semi-crystalline bulk polymer is blended with an amorphous immiscible matrix, a fine dispersion can be obtained (depending on the mixing conditions, rheology of the blend components and addition of compatibilizers) that can fulfill the previous condition. Then some MDs will be heterogeneity free, while others will contain heterogeneities.

The presence of several crystallization exoterms can be explained by considering that several groups of MDs can crystallize at different supercoolings, depending on the particular efficiency of the heterogeneities in promoting nucleation. Several types of heterogeneity may be present that are activated at different supercoolings. At larger supercoolings surface nucleation of clean droplets (i.e., heterogeneity free) may occur, or even homogeneous nucleation (at the largest possible supercooling that will be determined by the MDs volume).

We will present an example of fractionated crystallization behavior in immiscible blends where the matrix is constituted by amorphous PS and the dispersed phase is isotactic polypropylene (iPP) [36]. Fig. 3 presents standard DSC cooling behavior of the homopolymers and the 80/20 PS/iPP blend. The iPP crystallizes in one single peak located at 111 °C, on the other hand the PS shows its T_g at around 100 °C.

When PS and iPP are blended in an 80/20 proportion, the minor component (iPP) forms droplets of aprox. 1 μm in diameter dispersed in a PS matrix as revealed by SEM [36]. The number of iPP droplets (10^{11} particles/cm^3) is higher than the number of active heterogeneities in bulk iPP (i.e., 9×10^6 heterogeneities/cm^3 as determined by polarized optical microscopy in Ref. [36]).

The heterogeneities present in this commercial iPP do not have exactly the same efficiency and different kinds will be activated at different supercoolings. In bulk iPP, only the most active kind dominates the behavior causing the polymer to exhibit a single crystallization exotherm at low supercooling, as shown in Fig. 3. The less active heterogeneities do not have a chance to nucleate bulk iPP since once the most active heterogeneity triggers the formation of a certain nucleation density, the rest of the polymer crystallizes by secondary nucleation. The situation is changed when the polymer is finely dispersed into many MDs.

The iPP within the blend in Fig. 3 exhibits a fractionated crystallization characterized by four exotherms upon cooling from the melt (labeled A, B, C and D). Exotherm A occurs at the same supercooling as in bulk iPP and therefore can be attributed to the crystallization of a group of droplets that contain heterogeneity A, or the most active heterogeneity present in bulk iPP.

Exotherms B and C probably correspond to the crystallization of droplet populations that contain less active heterogeneities and therefore require higher supercoolings to nucleate. Finally, exotherm D can be attributed to the crystallization of clean MDs since it

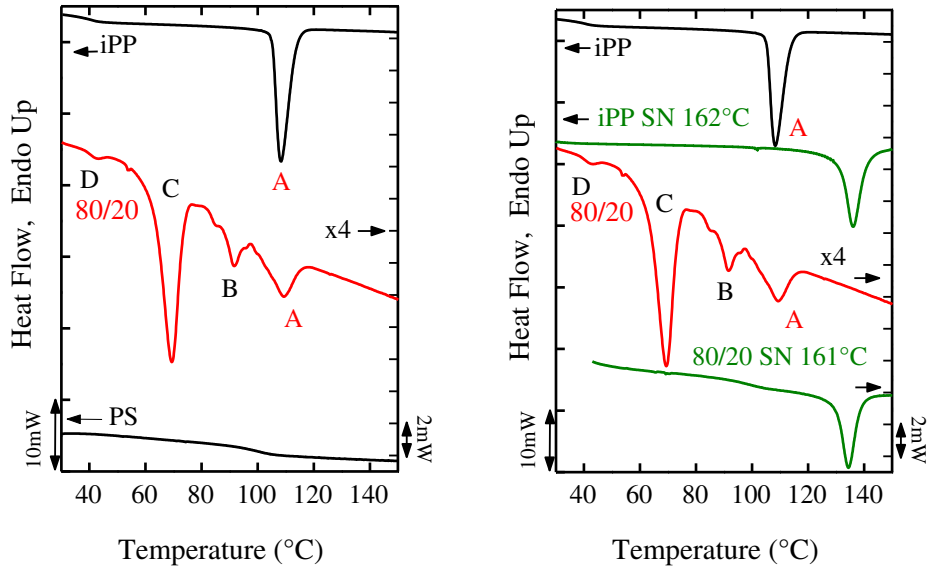

Fig. 3. Cooling scans at 10 °C/min for: (a) 80/20 PS/iPP blend and corresponding hompolymers, and (b) iPP and 80/20 PS/iPP blend before and after self-nucleation (data from Ref. [36]).

occurs at the largest supercooling. Since the crystallization temperature of exotherm D is still much higher than the T_g of iPP, it is unlikely that it corresponds to homogeneously nucleated crystals. It is therefore most probably due to the crystallization of droplets that were nucleated by surface nucleation.

The origin of fractionated crystallization is the lack of highly active heterogeneities in every MD present in the blend. If heterogeneous nuclei are injected in these MDs, then the fractionated crystallization should disappear and all the droplets should crystallize in a single step. Nuclei injection can be realized either by the addition of a nucleating agent or by the creation of self seeds through self-nucleation. Both strategies have been successfully applied in the past [36,73–79].

Fillon et al. designed an experimental protocol to induce self-nucleation within a semi-crystalline polymer by thermal treatments in DSC experiments where a sample with a standard crystallization history is partially melted to left self-nuclei that can increase the number density of nuclei by several orders of magnitude [80]. In order to demonstrate that the fractionated crystallization behavior shown in Fig. 3 is due to the lack of active nuclei in every MD, iPP was self-nucleated. The experiment was also performed in the homopolymer for comparison purposes. After self-nucleating iPP homopolymer at 162 °C (this was the ideal self-nucleation temperature, see Refs. [36,80,81]), the crystallization exotherm was shifted to much higher temperatures (a decrease in supercooling of 28 °C) as expected by the increase in nucleation density.

Fig. 3 shows how after self nucleating the iPP droplets in the 80/20 PS/iPP blend, the crystallization of all MDs now occurs at much higher temperatures in a single step. The peak crystallization temperature is about 4 °C lower than in the case of neat iPP, reflecting the fact that nuclei injection is more difficult than in bulk iPP (the ideal self-nucleation temperature was also 1 °C lower for the dispersed iPP).

Tol et al. [77,78,82,83] studied the crystallization behavior of a series of ternary blends composed by atactic polystyrene (PS), poly(phenylene oxide), PPE, and polyamide 6 (PA6). The PS and PPE are miscible with one another but they are immiscible with PA6. The crystallization of PA6 can then take place within a glassy or a rubbery matrix depending on the composition of the matrix, PS, PPE or PPE/PS blend. Hence, the authors were able to study the influence of the matrix, blend morphology, size and distribution of the dispersed phase on the crystallization of PA6. The most important results of the works of Tol et al. [77,78,82,83] are:

1. They corroborated previous findings (see Refs. [10,36] and references there in) indicating that fractionated crystallization depends on the relationship between the number of heterogeneities and the number of MDs. Fractionated crystallization only takes place if the number of MDs is the same or higher than the number of heterogeneities. The different peak crystallization temperatures of the several exotherms commonly observed correspond to different MDs populations containing different types of heterogeneities [10,36,73–76,84,85]. The thermal history of the sample can produce changes in the fractionated crystallization. A particular thermal treatment could change the morphology of the sample: changes from a co-continuous to a dispersed phase morphology will promote fractionated crystallization, while the reverse will cause its disappearance. The authors also corroborated that self-nucleation provokes enhanced nucleation of the sample in a single high temperature exotherm, as shown in Fig. 3 [10,36,73–76,84,85].
2. The nucleation density was found to be higher when the crystallization took place within a glassy matrix than in a molten or rubbery one.
3. Smaller droplets had slower crystallization kinetics and lower T_c values.
4. The crystallization kinetics showed higher temperature dependence for PA6 droplets in the blends than for bulk PA6. This difference could indicate that nucleation may be dominating the overall crystallization process. A similar phenomenon has been observed in crystallizable block copolymer components (see below and refs. [11,16]).
5. The crystals formed inside the dispersed MDs at higher supercoolings are highly metastable. An important difference between the crystallization enthalpy (during cooling scans) and the melting enthalpy (during heating scans) have been found for the systems studied by Tol et al. [77,78,82,83]. This behavior was due to crystal reorganization including lamellar thickening during the heating scans.

6. The confinement of PA6 within the blends led to changes in the type of crystals that were formed. Bulk PA6 developed α crystals, while PA6 droplets with size in the order of 1 μm preferentially formed γ phase crystals. Finally, the smallest droplets (less than one micron) exhibited crystals of the β form.

Fractionated crystallization has been usually observed in immiscible blends. However, several examples have also been reported for miscible blends. He et al. [86] studied the miscible poly (butylen succinate) (PBS) and poly(ethylene oxide) (PEO) blend. In the systems where the PEO is the minor component, the crystallization of PEO takes place at around −10 °C. The explanation is that PEO crystallizes in the confined space between PBS lamellae. In general, it is possible to have a confined environment within a miscible blend, if the polymers in the blend are both semicrystalline. Other conditions that must be satisfied are: (a) the polymer that crystallizes at higher temperatures should not be able to nucleate the minor component that crystallizes at lower temperatures, and (b) T_g values of both polymers must generally be different to allow different crystallization ranges.

The study of the crystallization kinetics in a blend exhibiting fractionated crystallization is very difficult. The reason being that the crystallization kinetics of each droplet population should be studied separately, at different crystallization temperatures, and the overlap of the different processes is almost inevitable. In some cases, however, when the blend morphology is extremely fine, a single crystallization exotherm at large supercoolings is observed, since the number of MDs can be several orders of magnitude larger than the number of available active heterogeneities. Hence statistically speaking, most of the produced droplets are heterogeneity free and can crystallize at very large supercoolings via surface or homogeneous nucleation.

One of such blends was recently studied by Cordova et al. [87], who were able to produce two types of very different blend morphologies by mixing PA6 (minor phase) with polyethylene. In one case (denoted MA) a fine sub-micron dispersion of PA6 droplets within a PE matrix was produced. On the other hand a second blend (denoted MC) was produced whose morphology was that of a co-continuous PA6 phase within a PE matrix. In both cases a single crystallization exotherm was obtained for the PA6 component upon cooling from the melt. The crystallization temperature of the PA6 component in the MC blend was much higher than in the MA blend (148.6 and 107.8 °C respectively), as expected for a percolated versus a confined phase.

When an ensemble of clean isolated micrometer or nanometer droplets or MDs are crystallized, their freezing temperatures will be much lower than the crystallization temperature for the same polymer in the bulk. This has several consequences from the overall kinetics of crystallization point of view. At such large supercoolings once a nucleus is formed (either by surface nucleation or homogenous nucleation), the MD crystallization will be almost instantaneous. Therefore, the slow step is the formation of the nuclei. This brings about a large change in the order of the crystallization kinetics. Polymers in bulk normally crystallize with sigmoidal type kinetics, usually described by an Avrami exponent of 3–4 (or even 2 in some cases). Once the nucleation is dominant, in the dispersed droplets case, the rate of isothermal overall crystallization kinetics is simply proportional to the fraction of droplets that have not crystallized and is therefore transformed to a first order kinetics or the equivalent to an Avrami index of 1 [21,25,88–90].

Fig. 4 shows a very clear example of the effect of the blend morphology (see also the TEM micrographs that appear as inserts) on the overall crystallization kinetics of the PA6 component within immiscible blends with PE. The overall crystallization kinetics exhibit an exponential dependence with time (typical of a first order kinetics) for the sub-micron droplet morphology of the MA sample. The "isothermal step crystallization" technique described in the experimental part (see below) was employed to collect the experimental data presented in Fig. 4a, since the usual continuous method was not sensitive enough [87]. On the other hand, when a blend of similar composition but with co-continuous morphology is studied, its crystallization kinetics exhibits a classical sigmoidal shape normally encountered in PA6 homopolymer.

Recently, an ingenious method to prepare nanolayers from a sequential coextrusion process has been introduced. In this method, the number of layers can be largely increased at the expense of reducing the thickness of the co-extruded layers. It is also feasible to obtain nanodroplets dispersions by annealing such multilayer coextruded ensemble. The following systems have been studied employing this method: polyethylene/polystyrene (PE/PS), polypropylene/polystyrene (PP/PS), polycarbonate/poly(ethylene terephtalate) (PC/PET) and poly(ethylene oxide)/ethylene acrilic acid copolymer (PEO/EAA). The crystallization behavior within the nanolayers and within the spheres that are obtained after heating and coalescence of the nanolayers have also been studied [45–54].

Wang et al. [53] and Pethe et al. [54] studied the crystallization of poly (ethylene oxide) (PEO) in a multilayer system of poly (ethylene oxide) co-extruded with an ethylene acrylic acid copolymer. They studied the crystallization in layers whose thickness varied between 3.6 μm and 8 nm. The orientation of the lamellae were random for 3.6 μm layers. By reducing the thickness to 20 nm, single lamellae were found in each PEO layer according to AFM, SAXS and WAXS results. In addition, the oxygen permeability was reduced by two orders of magnitude in the system that has PEO nanolayers with 20 nm thickness. Each PEO nanolayer contained a single large lateral lamella within it (i.e., a large PEO single crystal). The preparation of controlled thickness multilayer materials complements the potential of blends, thin films and block copolymers for the study of the phenomenon of crystallization in confined conditions.

Jin et al. [47–50] and Bernal-Lara et al. [46] studied the behavior of nanodroplets dispersions by annealing a multilayer coextruded ensemble of 257 thin layers formed by alternating PE or PP layers with immiscible PS layers. In the PP case, each thin PP film within the ensemble was approximately 12 nm thin. When the multilayer material was annealed, PP nanodroplets with sizes close to 30 nm were formed. They found crystallization temperatures of around 40 °C and have attributed this high supercooling as compared to the bulk polymer to homogeneously nucleated crystal formation. However, no evidences were presented to disregard other possibilities like surface nucleation. Their WAXS results indicate that the PP is crystallizing in a smectic phase within the nanodroplets. This type of crystallographic arrangement could be a consequence of the way the nanodroplets are prepared, since they come from the rupture and coalescence of nanolayers and therefore in agreement with the recent observation of Kailas et al. [38] who found similar results for droplets whose thickness were below 5 nm (see above). On the other hand, Arnal et al. [76] obtained PP droplets in the micron range (1–2 μm) in a PS matrix (by melt blending) and demonstrated by WAXS that the droplets crystallized in the typical α phase of PP, just as the bulk polymer. Clearly, the size of the droplets has an important influence on whether the smectic PP phase develops or not.

Jin et al. [47–50] studied the effect of adding nucleating agents to multilayered thin film ensembles containing PP. After annealing the ensemble to prepare droplets of PP in a PS matrix, the exotherm at 40 °C which was attributed to homogeneously nucleated crystallization decreased in size when sorbitol was used as a nucleating agent. This result corroborates earlier findings by Santana and Müller who reported the complete disappearance of fractionated

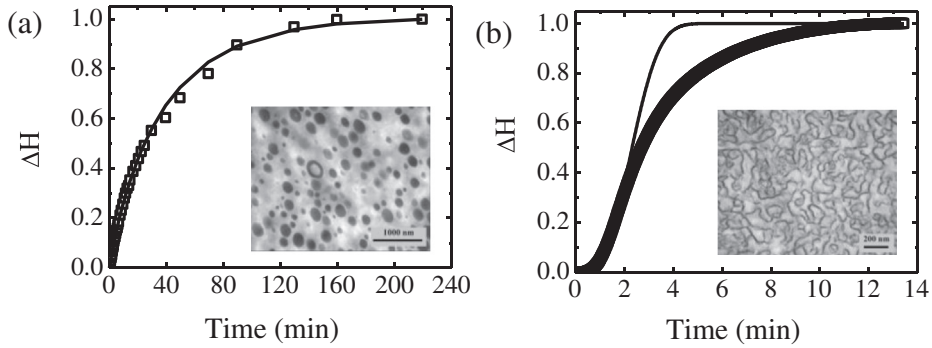

Fig. 4. Variation of PA6 component relative degree of crystallinity (expressed as relative ΔH values) with time for (a) PA6/PE blends with a submicron droplet morphology (MA) (T_c = 102.5 °C) and (b) with a co-continuous morphology (MC) (T_c = 166 °C). Solid lines represent fittings to the Avrami theory. The inserts show TEM micrographs that reveal the blend morphology. Data taken from Ref. [87].

crystallization of PP droplets in a PS matrix when the nucleating agent phtalocyanine blue was added to the blend [73].

4. Block copolymer crystallization

Block copolymers in the strong segregation regime may exhibit morphologies where MDs can be isolated and independent of one another, and in consequence the crystallizable blocks may exhibit fractionated crystallization or exclusive crystallization of heterogeneity free MDs at large supercoolings. The formation of segregated MDs in block copolymers is a function of the composition of the block copolymer and the segregation strength between the blocks, given by χN, where χ is the Flory–Huggins interaction parameter between the constituent blocks and N the polymerization degree of the copolymer [91–93]. Additionally, three important temperatures must be considered in the case of a linear diblock copolymer composed of an amorphous block and a semi-crystalline block: the order-disorder temperature (T_{ODT}), the crystallization temperature (T_c) of the semi-cristalline block and the glass transition (T_g) of the amorphous block [11–13,16,17,93]. Table 1 summarizes the different morphologies that could be expected when dealing with a relatively simple linear diblock copolymer system.

If the diblock copolymer is in the strong segregation limit, crystallization has to occur within the confined MDs that are typically formed depending on composition: lamellae, gyroids, cylinders or spheres. Although the morphologies remain almost intact, some level of distortion may occur in view of the densification process that accompanies crystallization [11].

In a previous review [11] examples of all the cases given in Table 1 can be found. More complicated systems where both blocks can crystallize [14–16] or when the copolymer presents more complex molecular architectures have also been examined in the literature (like ABC triblock terpolymers or myktoarm stars) [11,16,94]. Also, the influence of the interphase on polymer crystallization within block copolymers has been studied [95]. The interested reader is referred to recent reviews on the subject of block copolymer crystallization [11–17].

In this section, we will focus on the confined crystallization of poly(ethylene oxide), PEO, within poly(ethylene oxide)-*b*-polybutadiene diblock copolymers, PEO-*b*-PB, since we will also deal in the next section with the infiltration of PEO within alumina nanopores and its confined crystallization in a hybrid material. We will also present a less frequently reported case of confined block copolymer component crystallization within a miscible block copolymer system.

Castillo et al. recently studied the crystallization and melting of the PEO block within PB-*b*-PEO linear diblock copolymers prepared by living anionic polymerization [96]. Two copolymers with low PEO content were studied: $B_{81}EO_{19}^{34}$ and $B_{89}EO_{11}^{105}$, where the subscripts correspond to the composition in wt.% and the superscripts to the number average molecular weight given in kg/mol. The calculated values of χN for these block copolymers are higher than 50, in consequence they are strongly segregated within a soft environment since PEO will crystallize upon cooling when the PB block is rubbery (the T_g of the PB block is around −70 °C).

The morphology was determined by TEM and SAXS. $B_{89}EO_{11}^{105}$ exhibited a morphology of PEO nanospheres randomly dispersed in a PB matrix. On the other hand, $B_{81}EO_{19}^{34}$ presented a mixed morphology of short cylinders and spheres, since its composition is close to the cylinder–sphere transition, and both morphologies were present but with a clear preference to sphere formation. As expected the size of the domains of the $B_{81}EO_{19}^{34}$ are larger than in $B_{89}EO_{11}^{105}$. In both cases the size of the spheres are in agreement with the values reported previously in other similar systems [88,97–99].

Fig. 5 shows DSC cooling and heating scans for $B_{81}EO_{19}^{34}$ and $B_{89}EO_{11}^{105}$ diblock copolymers. During cooling three and two exotherms are observed for $B_{81}EO_{19}^{34}$ and $B_{89}EO_{11}^{105}$ respectively.

Table 1
Possible morphologies of a linear diblock copolymer with one crystallizable block depending on the segregation strength and T_{ODT}, T_g and T_c values.

Segregation level	$T_{ODT}/T_g/T_c$	Morphology in the solid state
Homogeneous melt	$T_{ODT} < T_c > T_g$	Crystalline lamellae surrounded by amorphous material
Weakly segregated systems (low χN values)	$T_{ODT} > T_c > T_g$	The crystallization destroys previous melt structure (by break-out) and crystalline lamellae are formed.
Medium segregated systems (medium χN values)	$T_{ODT} > T_c > T_g$	Quenching: the melt segregated morphology is preserved. Slow cooling: Break-out and crystalline lamellae are formed.
Strongly segregated systems (high χN values)	$T_{ODT} > T_c > T_g$	The crystallization can be confined within the MDs dispersed in a rubbery block matrix (soft confinement)
	$T_{ODT} > T_g > T_c$	A strictly confined crystallization within the MDs dispersed in a glassy matrix (hard confinement)

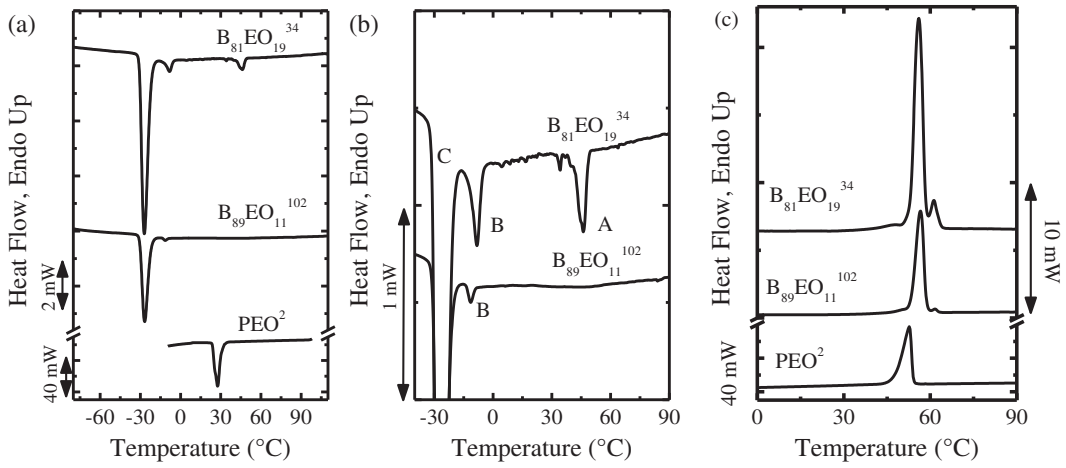

Fig. 5. DSC cooling (a) and (b) and heating (c) scans at 20 °C/min for the $B_{89}EO_{19}^{34}$ and $B_{89}EO_{11}^{102}$ block copolymers. A PEO homopolymer is shown for comparison purposes. Data taken from Ref. [96].

These exotherms correspond to the fractionated crystallization of the PEO MDs. The number of MDs estimated by TEM by Castillo et al. [96] for $B_{89}EO_{11}^{105}$ was about 10^{16} spheres/cm^3, while the number of highly active heterogeneities in PEO is around 10^6 heterogeneities/cm^3. Hence, the majority of the MDs will be heterogeneity free.

In the case of $B_{81}EO_{19}^{34}$ the mixed morphology between cylinders and spheres also contains percolation between a small number of these MDs. This is the reason why, in this block copolymer, a small exotherm (labeled A) was obtained (see Fig. 5a) whose peak crystallization temperature is the same as that of neat PEO. Therefore, the small number of percolated MDs crystallized by heterogeneous nucleation. The second exotherm (labeled B) upon cooling from the melt possibly originates in the crystallization of a group of MDs that contain a less active type of heterogeneities. Finally, the exotherm encountered at the largest supercooling (labeled C) is most probably due to the crystallization of heterogeneity free MDs.

In the case of the copolymer with only 11% of PEO, the morphology is dominated by isolated spheres. This is reflected in the absence of the exotherm labeled A in Fig. 5a. In fact, most of the spheres crystallize in exotherm C, where heterogeneity free MDs crystallize at the largest supercooling.

For both block copolymers, the dominant crystallization of clean MDs occurs in a temperature range that although is very low (at around −25 °C) as compared to PEO homopolymer (which crystallizes at temperatures that are nearly 50 °C higher), it does not correspond to the homogenous nucleation temperature reported for MDs of similar volume [11,100] that crystallize at even lower temperatures (aprox. -45 °C). Therefore, the nucleation of the MDs that crystallize in exotherm C (Fig. 5a) was initiated at the surface or the interphase with the PB block [11,96,100].

Usually the reorganization of the crystals formed at extreme supercoolings during the subsequent heating scan originates a single melting endotherm (see Refs. [11,16,36,75,84,100–102]), however in the systems studied by Castillo et al. [96] a fractionated melting was reported for the first time. A complex series of annealing and isothermal crystallization experiments were performed in order to establish the origin of the multiple melting peaks which were related to the fractionated crystallization of the samples (see Ref. [96] for more details).

Castillo et al. [96] also studied the isothermal crystallization kinetics of the copolymers. They performed the experiments by the isothermal step crystallization procedure (similar to that described in the experimental part of this paper) and the data was fitted with the Avrami equation. The isothermal analysis at low temperatures, corresponding to the crystallization of the isolated MDs, resulted in Avrami indexes around 1 (the reported values were: 1.27, 1.01, 0.96). These results were expected, since as in the PA6 droplets within the polymer blends case (Fig. 4a), the nucleation dominates the overall crystallization process of these isolated and heterogeneity free PEO nanodomains.

In the case of crystallizable block copolymers, a clear correlation between the Avrami index and the morphology has been demonstrated (see Refs. [11,13–16,94] and references therein). The Avrami index decreases as confinement increases. In the case of morphologies where the crystallizable polymer can percolate throughout the material and therefore spread the crystallization by secondary nucleation, the Avrami index reflects the dimensionality of growth (usually two or three dimensions) and the nucleation kinetics (from instantaneous to sporadic). However, when the MDs are truly isolated, like in the case of well developed cylinders and spheres, the nucleation can dominate the behavior and the Avrami index will typically be 1 or even lower (see Refs. [11,13–16,94] and references therein).

As well as in blends, confinement can also be present in miscible block copolymers, although it is not so common as in strongly segregated systems. When a miscible double crystalline diblock copolymer crystallizes from a mixed melt, the first block to crystallize usually templates the morphology (e.g., by forming spherulites) leaving interlamellar regions filled with amorphous chains (from both components) that upon further cooling provide the spatial confinement where the second block must crystallize [14,15].

In the case of a miscible PA6-*b*-PCL (with 52% PCL and a total molecular weight of 6.700 g/mol) block copolymer, the crystallization of the PCL block is confined between the crystalline PA6 lamellae that formed at higher temperatures [103]. The crystallization exotherm for the PCL block was impossible to detect in a cooling scan in a DSC at 20 °C/min, however the block was able to crystallize since a melting peak corresponding to the PCL block was detected during a subsequent heating run (see Fig. 6a). The samples were studied employing the isothermal step crystallization technique. Fig. 6b shows how the shape of the relative ΔH versus time curve changes from the classical sigmoidal shape for bulk PCL, to a simple first order exponential growth in the block copolymer. The Avrami equation was employed to fit the data and the Avrami index was very low for the confined PCL in the copolymer, i.e., between 0.4 and 0.8 [103].

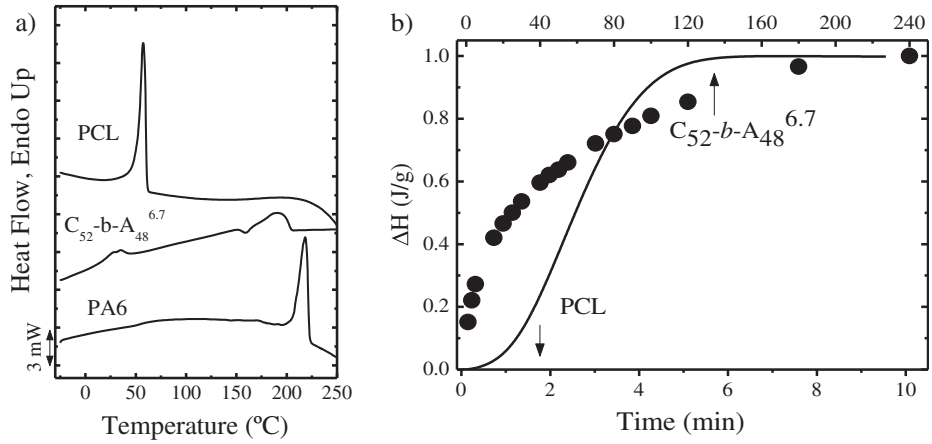

Fig. 6. a) DSC heating scans at 20 °C/min of a PCL-*b*-PA6 block copolymer (C_{52}-*b*-$A_{48}^{6.7}$) and its corresponding homopolymers. b) Variation of the relative degree of crystallinity (expressed as relative ΔH values) with time for PCL homopolymer and the PCL component within C_{52}-*b*-A_{48}^{6} diblock copolymer [103].

5. Crystallization within nanostructures formed from solutions

The use of copolymers in solution is very common, especially when one of the blocks is preferentially dissolved by the solvent employed, in those cases the formation of nanostructures are expected. If the insoluble block is semicrystalline, the crystallization will take place in a confined environment, a reduction of T_m and T_c has been reported for these systems [104,105]. The shape of the nanostructure depends not only on the traditional variables, like molecular weight, composition or segregation strength, but in this case the solvent plays a very important role. For block copolymers to self-assemble in these conditions, the solution must be heated above the T_m of the semicrystalline block so that during cooling crystallization and hence the formation of the nanostructure takes place [104–141].

Weber et al., and Rochette et al. [44,142] have reported the synthesis, nano-structuring and crystallization of polyethylene in water. They employed surfactants in order to stabilize the remarkable nanostructures that can form in water. Inside the nanostructures (known as nano-hamburgers by their peculiar morphology) a single lamella was sandwiched between two layers of amorphous polyethylene. They found very large supercoolings which are in agreement with the confined environment of the nanoparticles [44]. Additionally, they studied the effect of lamellar thickening produced by annealing lamellae formed inside the produced nanostructures [142].

Another important consequence of the crystallization at extreme supercoolings produced by confinement is the creation of highly metastable polymeric crystals that upon heating will need to reorganize. This subject has been studied in detailed both in PEO nanospheres within block copolymers by Röttele et al. [97,143] and in sub-micrometer PA6 droplets by Tol et al. [144].

6. Crystallization within anodic aluminum oxide templates

6.1. Experimental part

6.1.1. Materials

The samples employed in this work are: (a) A polyethylene oxide sample from Scientific Polymer Products with a number average molecular weight (M_n) of 100 kg/mol (EO_{100}^{100}) and a polydispersity index of approximately 3, and (b) A poly(ethylene oxide) -*block*- poly(1,4-butadiene) diblock copolymer (Bd_{21}-*b*-EO_{79}^{257}) with a composition of 79 wt.% of PEO and 21 wt.% of PB and M_n equal to 257 kg/mol and a polydispersity index of 1.1. This copolymer was generously supplied by the group of Prof. Nikos Hadjichristidis and was synthesized by living anionic polymerization (see acknowledgements).

6.1.1.1. Infiltration. The AAO templates employed in this work had an average diameter of 35 and 60 nm and pore lengths of approximately 100 μm. They were prepared by the two-step anodization method as reported elsewhere [145]. For that, the AAO templates were first cleaned with solvents of different polarity (water, ethanol, and acetone) and then electro-polished. Subsequently, a first anodization is performed in an acidic electrolyte under constant voltage, the first alumina layer is dissolved, and then the second anodization is carried out.

The precursor film wetting method was used for infiltrating both samples (EO_{100}^{100} and Bd_{21}-*b*-EO_{79}^{257}). The polymers were heated to a temperature well above the melting point (T_m) during the infiltration. First, the AAO templates were annealed at 200 °C in vacuum in order to remove the possible adsorbed organic molecules from the pore walls. Copolymer infiltration into two alumina templates with 35 and 60 nm diameter pores was carried out by placing the solid materials onto the AAO at 117.5 °C and then annealed under a nitrogen atmosphere for 3 h to be sure that the copolymers will not degrade but, on the other hand, all the pores will be infiltrated. In the case of homopolymer the temperature of infiltration was 107.5 °C with time of infiltration 1.5 h. After the infiltration process, the samples were quenched under ice-water and finally cleaned with the aid of a blade to remove any remaining polymer on the surface.

6.1.2. Differential scanning calorimetry

6.1.2.1. Standard DSC measurements. Samples of templates with infiltrated EO_{100}^{100} weighing 70 mg were employed. These samples contained the precursor aluminum at the bottom of the template, plus the alumina template and the infiltrated polymer. The exact mass of infiltrated polymer is unknown but has been estimated by TGA to be of the order of 1% of the total weight of the sample (circa 0.7 mg). In the case of the infiltrated Bd_{21}-*b*-EO_{79}^{257}, the aluminum base was removed and 25 mg were employed consisting of just alumina template and the infiltrated copolymer. From these about 0.25–0.5 mg correspond to the copolymer sample. The samples were encapsulated in hermetically sealed 100 μL Aluminum pans.

DSC standard runs were performed on a Diamond Perkin Elmer Instrument at 20 °C/min calibrated with zinc and indium under an

ultra high purity nitrogen atmosphere. The results obtained with the infiltrated samples were compared with neat samples at the same scan rates and employing a mass of 5 mg.

6.1.2.2. Isothermal DSC experiments. Two methods were employed to perform the isothermal crystallization kinetics employing DSC: the conventional or "continuous isothermal crystallization" [146] and the "isothermal step crystallization" technique [147].

The conventional or "continuous isothermal crystallization" experiments were performed to the un-infiltrated samples. After erasing the crystalline history of the samples by heating them for 3 min at 25 °C above the melting temperature, the samples were quickly cooled (at a controlled rate of 60 °C/min) to a crystallization temperature (T_c) at which the isothermal DSC scan was recorded. Experimental checks were performed to ensure that the sample did not crystallize during the cooling to T_c (by heating the samples immediately after reaching the corresponding T_c values and ensuring that no melting was observed, see Ref. [146]).

In the case of the infiltrated samples within the alumina templates, the crystallization of the confined nanocylinders (inside the alumina nanopores) was impossible to detect by standard isothermal crystallization experiments. The reason is that the heat evolved per unit time is too small to be detected by the calorimeter in isothermal mode.

The isothermal crystallization of the polymers infiltrated in the alumina templates was determined with a technique employed previously with block copolymer microphases termed "isothermal step crystallization" [147]. A similar technique has also been used before by Galante et al. [148] The procedure involved the following steps: (a) erasure of crystalline history by heating the sample to 25 °C above the melting temperature for 3 min; (b) fast cooling (at a controlled rate of 60 °C/min) down to T_c; (c) the sample was held at T_c for a time t_c which was later increased in the subsequent steps; (d) heating at 20 °C/min from T_c to 25 °C above the melting temperature. The heat of fusion calculated from this DSC heating scan should correspond to the crystallization enthalpy of the crystals formed in step "c" at T_c for the specified crystallization time; (e) steps "a"–"d" were repeated employing the same T_c in step "b", but increasing t_c. The final t_c was taken as the time the melting enthalpy in the subsequent heating scan did not change with respect to the previous one; (f) the whole process was repeated for different T_c temperatures.

Anodic aluminum oxide (AAO) templates were first prepared by Massuda et al. [149]. Aluminum is submitted to a double anodization process. During the first one, an irregular AAO layer is formed, this layer is removed and in the second anodization a hexagonally porous array of AAO is obtained (see Fig. 7). Depending on the conditions employed during template preparation, different pore sizes could be achieved (for detail information on template preparation see Ref. [150,145]).

Once the template is prepared, the infiltration of a polymeric material into the nanopores is possible. Different methods can be used to infiltrate the polymer. One of the most employed is melt infiltration, were a film of polymeric material is placed on the top of the pores and melted. The molten polymer fill the pores after a time has elapsed (for detail information on the infiltration methods and filling process, see Ref. [150]). This process is also known as nanomolding [151–155]. In some cases, an interconnecting layer remains on the top of the template, this layer must be removed in order to appreciate a truly confined behavior of the nanodomains within the nanopores of the templates. Also the polymer can be extracted from the template after infiltration, in order to obtain nanofibers or nanocylinders.

The crystallization of polymers within AAO templates has attracted much recent attention [37,145,156–169]. Several general trends can be extracted from a review of the literature:

1. The crystallization temperature (T_c) decreases with pore size. Woo et al. [163] studied the crystallization of linear polyethylene (PE) infiltrated in AAO templates. Several pore sizes were studied, from 15 to 110 nm. Fig. 8 shows the variation of the minimum crystallization temperature. These temperatures

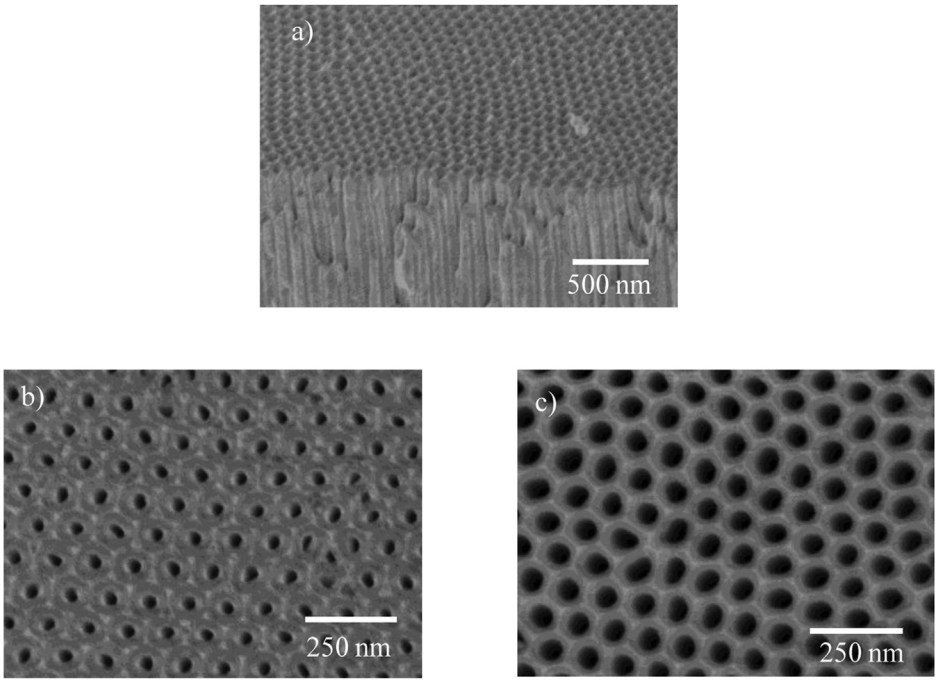

Fig. 7. SEM micrographs of prepared AAO templates: (a) 35 nm side view, (b) 35 nm top view, (c) 60 nm top view.

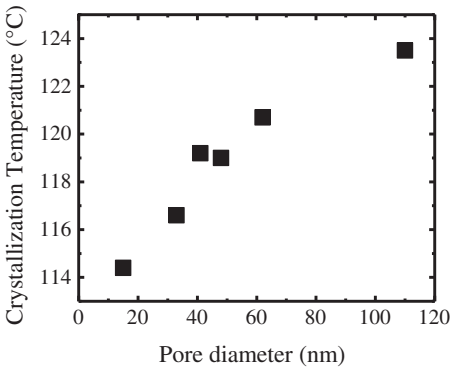

Fig. 8. Minimum crystallization temperature versus de pore diameter for the PE infiltrated in AAO templates (Data extracted from Ref. [163]).

are too high to correspond to homogenous nucleation of PE (see Refs. [11,16,34,36,37]) and their origin must be related to either surface nucleation or nucleation induced by the AAO walls.

Similar results of decreasing crystallization temperatures with pore sizes have been found for infiltrated PP [156], PEO [37,167,170] and PE-*b*-PS [37] copolymers.

2. The degree of crystallinity is generally lower for infiltrated polymers within AAO nanopores than for neat polymers in the bulk state [156,157,167]. Similar results have been obtained for crystallizable MDs within block copolymers and blends (see Refs. [11,16] and references there in).
3. Depending on the pore size and the number of highly active heterogeneities, it is possible to observe fractionated crystallization of infiltrated polymers. In this case the presence of traces of the film employed during the infiltration process may lead to the presence of an additional exotherm at the same undercooling as in the neat polymer, in view of the percolating path connecting a series of nanopores. Fig. 9 shows a cooling scan of EO^{100} (see experimental part) infiltrated within a 35 nm AAO template prepared in this work, that contained some traces of the interconnecting PEO film (remaining from the infiltration procedure, which was not completely removed) and after carefully removing it. In the sample with the interconnecting PEO layer a fractionated crystallization process with three crystallization peaks was detected. Once the layer is completely removed, only the crystallization peak at maximum supercooling was observed.
4. The melting temperature also changes with pore diameter (see Fig. 10). This behavior is especially noticeable at small pore sizes, were the lamellae are forced to be thinner due to a reduction in the space available to crystallize.
5. The chain in the crystals, inside the nanopore, is usually oriented perpendicular to the cylinder axis (see Fig. 11). In block copolymers with cylindrical nanodomains the orientation of the chain is a function of the supercooling employed. At medium supercoolings the chain is perpendicular to the cylinder axis [171–176]. Studies made on linear PE [157], PEO [37], Poly(vinylidene difluoride) (PVDF) [158,161,162] and syndiotactic polystyrene (sPS) [164,165] found that chains in the crystals are perpendicular to the pore axis. However, Steinhart et al. [161] found a dependence of the interconnecting layer (the film remaining from the infiltration that can provide a percolation path between the nanopores) and the chain orientation. If this layer remains on top of the nanopores, the crystals grew in the fastest direction, and the chain was perpendicular to the pore axis. On the other hand, if the nanodomains were isolated, no preferential orientation was observed [161]. In the case of the sPS studied by Wu et al. [164], two different orientations depending on the size of the nanopore were found. At larger nanopore diameters, the preferential orientation was perpendicular to the pore axis, however, at increasingly smaller pore diameters the chains eventually crystallized parallel to the nanopores. A similar result has been recently found for PEO infiltrated in AAO templates [177]. It would seem that for pore sizes exceeding 25 nm, most of the works published have found a perpendicular orientation of the chains inside the nanopores, since this facilitates crystal growth (Fig. 11).
6. Confinement inside nanopores can induce changes in polymorphism, as reported for Poly(vinylidene fluoride-co-trifluoroethylene) within AAO pores [160]. Wu et al. also found modifications on the crystal structure of sPS crystals, from β phase found in the bulk to α upon infiltration [159,165]. On the other hand, PVDF changes from α to γ after infiltration [158]. Less dramatic changes were shown by Polyaniline (PANI), since in this case, the infiltration modifies the crystal unit cell from orthorrombic to pseudo-orthorrombic [178].
7. Double confinement can cause further reductions in crystallization temperature, as reported by us when PS-*b*-PE strongly segregated diblock copolymers were infiltrated in AOO nanopores. A diblock copolymer containing a PS matrix and already confined PE cylinders was infiltrated into AOO nanopores and a phenomenon of double confinement was reported, since the PE

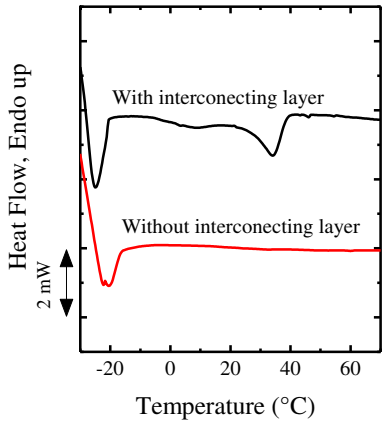

Fig. 9. Cooling DSC scans for PEO^{100} infiltrated in this work within a 35 nm AOO template.

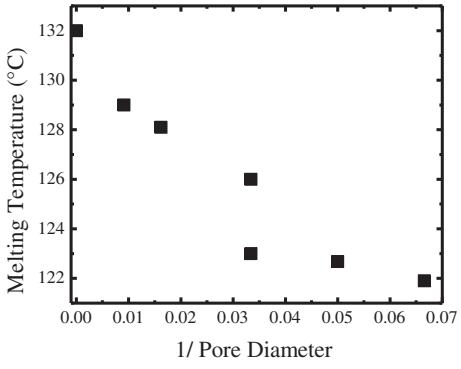

Fig. 10. Variation of the melting temperature with the inverse of the pore diameter [157].

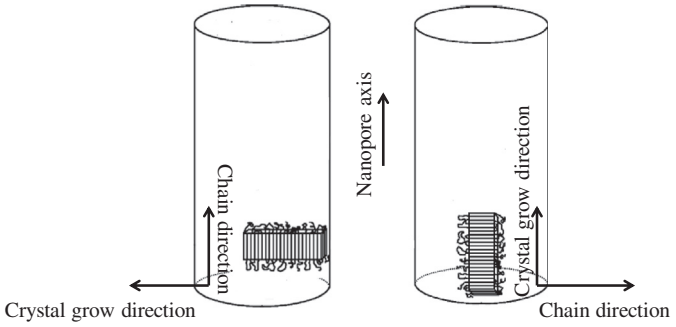

Fig. 11. Graphical representation of the possible crystal orientation within AAO nanopores [164].

block experienced the confinement of the PS vitreous block covalently bonded to it plus that caused by the inorganic AOO walls. The PE block (as well as PE homopolymer infiltrated for comparison purposes) crystallization was started by surface nucleation [37].

Most of the studies that have been published so far on the confined polymer crystallization within AAO templates, have focused on crystal orientation, changes in crystalline morphology and the influence of the nanopore size on the crystallization temperature, melting and crystallinity degree [37,145,156–167,170,179–182]. However, the study of isothermal crystallization kinetics has been limited to a few papers [156,157,163,170]. In most cases, the Avrami Indexes reported are larger than 1, which are unexpected values.

As reported above, it has been extensively documented in the literature that an ensemble of isolated and confined MDs that are free from heterogeneities normally crystallize at much larger supercoolings than the bulk polymer and typically exhibit a first order nucleation kinetics (or lower order), that corresponds to an Avrami index of 1 (or lower than 1). This behavior has been reported for both surface nucleation (see Figs. 4 and 6) and homogeneous nucleation in droplets, blends and block copolymers [11,13,16,24,25,87–90,96,100,103,147,174]. We present new results on the thermal properties of PEO and PBd-*b*-PEO before and after infiltration in AAO templates. We found the typical behavior of confined polymers with respect to their crystallization kinetics and thermal properties. The results obtained after performing standard DSC tests are shown in Fig. 12.

The results shown by un-infiltrated PEO is the typical behavior of a standard DSC test of a semi-crystalline homopolymer. Both melting and crystallization temperatures are within the expected range (see Table 2). The Bd_{21}-*b*-EO_{79}^{257} block copolymer exhibits a morphology of PB cylinders inside a PEO matrix [96]. It must be noted that the PEO block is of a narrow molecular weight distribution, while the commercial PEO homopolymer used for comparison purposes is polydisperse. As a result, the values of T_c differ by 3 °C (see Table 2).

According to the results shown in Fig. 12 and Table 2, it can be observed that confinement caused a dramatic reduction of the crystallization temperature. In the case of the PEO homopolymer infiltrated in a 35 nm template, the reduction in T_c value was of 65.0 °C in agreement with a previous work by us with a different PEO sample [37]. A similar behavior has been reported for PEO and also for other polymers that have been infiltrated in nanopores, like PP, PE, sPS and PVDF [37,156–165]. In the case of Bd_{21}-*b*-EO_{79}^{257} diblock copolymer within a 35 nm AAO template, the crystallization temperature of the PEO block changed from 46.2 °C in the bulk to −26.0° C in the template, or a reduction of 72.2 °C. Such low crystallization temperatures for PEO are characteristic of heterogeneity free MDs (for the volume of the PEO nanocylinders inside the AOO pores). In fact, the number of nanopores in the templates is approximately 10 orders of magnitude higher than the number of active heterogeneities in bulk PEO, therefore, the number of clean MDs will be exceedingly higher than those with heterogeneities. The question is whether or not crystallization started from homogeneous nuclei within the volume of the nanopores or was triggered by the AAO surface in contact with the polymer. In the case of homogeneous nucleation, the crystallization temperature should occur at very large supercoolings (close to vitrification) and should be a function of the MDs volume. [11,35,37,88].

Müller et al. [11] collected information from various PEO confined systems where homogeneous nucleation was found. From

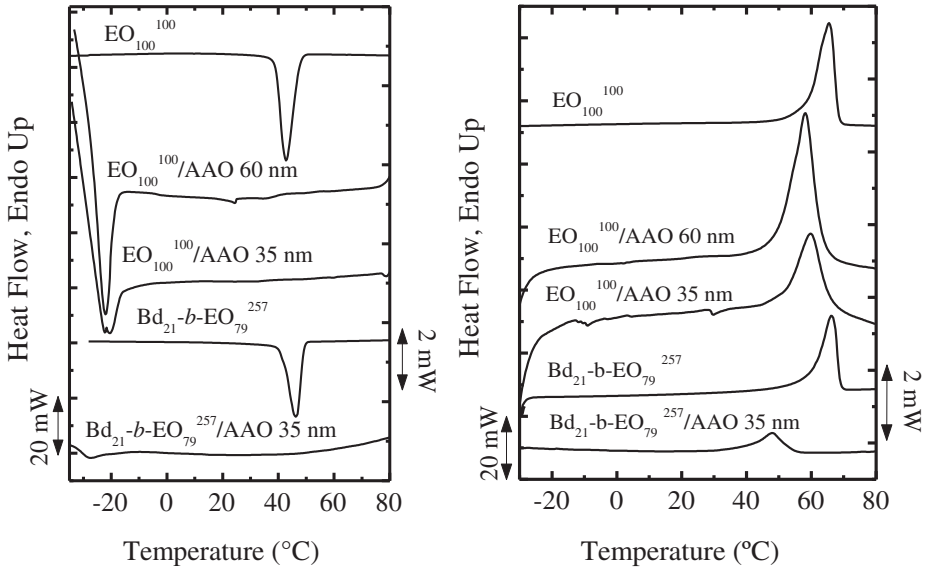

Fig. 12. DSC cooling (left) and heating (right) scans for the indicated samples. The *y*-axis scale on the left of the plots (i.e., 20 mW) corresponds to the un-infiltrated neat materials, while that on the right (2 mW) corresponds to the AAO infiltrated materials.

Table 2
Transition temperatures and enthalpies obtained by DSC standard heating and cooling scans.

Sample	T_c (°C)	ΔH_c (J/g)	T_m (°C)	ΔH_m (J/g)
EO_{100}^{100}	42.7	−127	65.5	135
EO_{100}^{100}/AAO 60 nm	−22.1	−0.7*	58.3	1.6*
EO_{100}^{100}/AAO 35 nm	−22.3	−0.3*	59.7	0.8*
Bd_{21}-*b*-EO_{79}^{257}	46.2	−111	66.1	122
Bd_{21}-*b*-EO_{79}^{257}/AAO 35 nm	−26.0	−0.5*	50.8	0.6*

Non-normalized, because the exact weight of the polymer inside the nanopores is unknown.

these data an empirical relationship between the volume of the MDs and the crystallization temperature for PEO was proposed:

$$T_c = -41.8 + 2.89\log(v_d) \quad (1)$$

where T_c is the crystallization temperature of the PEO MDs and v_d corresponds to their average volume. If we calculate the volume of the PEO nanocylinders inside the templates and apply equation (1), the expected homogeneous nucleation temperature for the PEO nanocylinders can be calculated. These temperatures are −19 °C and −17 °C for the templates with 35 and 60 nm respectively. Comparing these values with those experimentally found by DSC tests (−22 °C for both cases), a homogeneous nucleation process is highly probable in these two cases.

For the block copolymer it is not possible to determine exactly the phase volume of PEO, since the morphology of the block copolymer may have change with infiltration, as has been reported for other block copolymers in the literature [183–185]. However, we can speculate that in any case, the volume occupied by the PEO should be lower than the size of the nanopore, therefore the crystallization temperature for this system should be lower than the crystallization temperature of the infiltrated PEO homopolymer. In fact the temperature reported in Table 2 for the PEO block within the infiltrated block copolymer is lower (−26 °C) than for neat infiltrated PEO. Therefore, we believe that the nucleation of the PEO nanodomains was homogeneous.

For the PEO two different template diameters were employed. An increase of the crystallization temperature with pore diameter has been reported for several infiltrated polymers [37,156,162–165]. However the difference in pore volume employed here was not large enough to generate significant differences in crystallization temperature.

If the nucleation of the infiltrated MDs was indeed homogeneous, a first order crystallization kinetics would be expected. In the case of the infiltrated samples, the measurements of the overall isothermal crystallization kinetics were performed employing the DSC based step crystallization technique (as detailed in the experimental part).

The results of the isothermal crystallization experiments are shown in Figs. 13 and 14. Fig. 13 shows the relationship between the relative degree of crystallinity ΔH and time for samples before and after infiltration. In the case of un-infiltrated PEO and Bd_{21}-*b*-EO_{79}^{271} the isotherms display a typical sigmoidal shape, as expected for polymers free from confinement. After infiltration a dramatic change is observed, since the curve corresponds to a simple

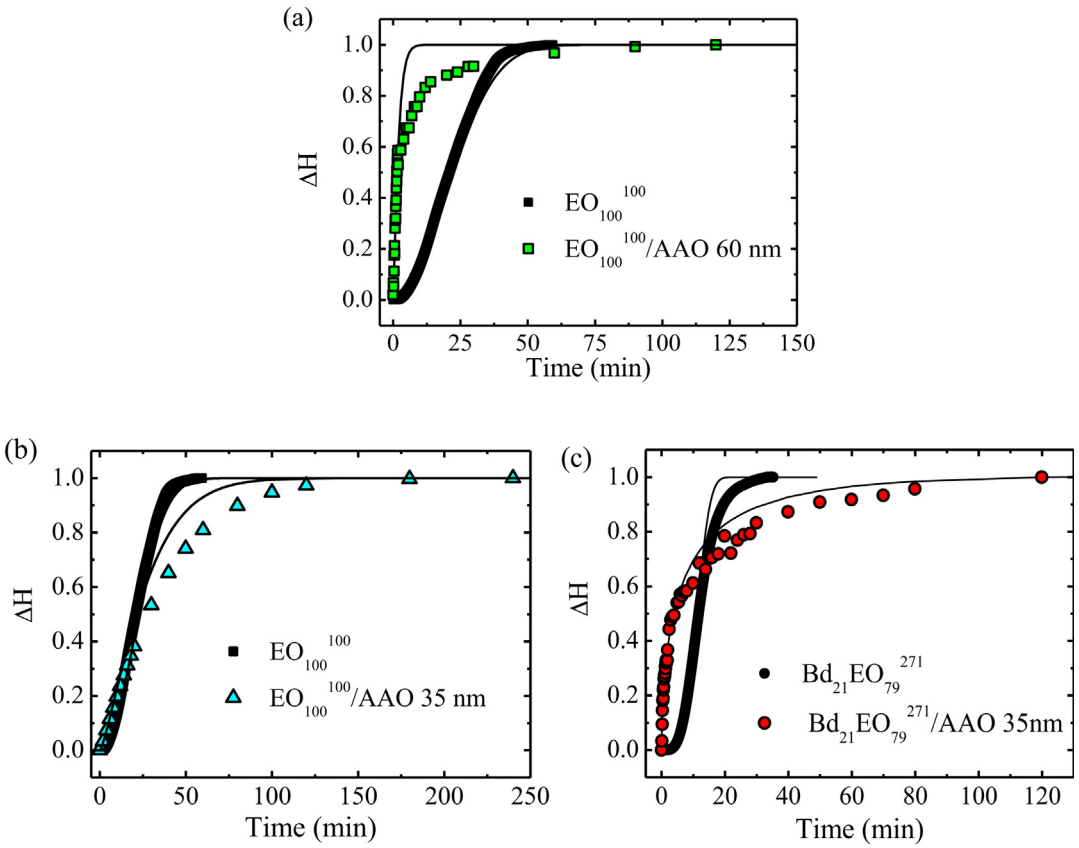

Fig. 13. Variation of the relative degree of crystallinity (expressed as relative ΔH values) with time for (a) EO_{100}^{100} in the bulk (T_c = 54 °C) and within a 60 nm AAO template (T_c = −4 °C), (b) EO_{100}^{100} in the bulk (T_c = 54 °C) and within a 35 nm AAO template (T_c = −8 °C), (c) Bd_{21}-*b*-EO_{79}^{257} in the bulk (T_c = 58 °C) and within a 35 nm AAO template (T_c = −4 °C). The solid lines represent fits to the Avrami equation.

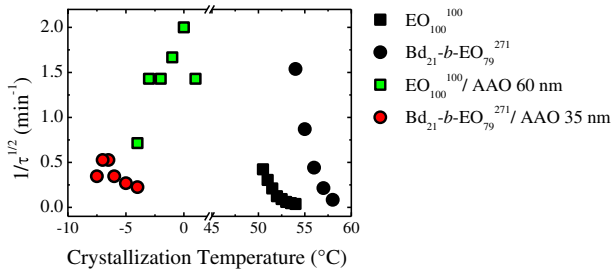

Fig. 14. Inverse of $\tau^{1/2}$ experimental values versus crystallization temperature for the indicated samples.

exponential growth, with a crystallization kinetics very close to being first order (as will be apparent from the Avrami indexes presented below). This trend was observed for all the infiltrated samples at all temperatures studied.

Fig. 14 shows that the infiltrated samples require a much larger supercooling to crystallize, this difference is attributable to the higher energy barrier needed to activate homogeneous nuclei. Because the calorimetric signal measured in the infiltrated materials was very small, measurements at low conversion times were repeated at least three times. Despite these considerations, the experimentally determined half-crystallization times ($1/\tau^{1/2}{}_{exp}$) values, shown in Fig. 14 for the infiltrated material, show some dispersion. In addition, in the case of the infiltrated EO_{100}^{100} within a 35 nm template, the crystallization signal was too small for accurate measurements to be collected except in the case of one crystallization temperature (see Table 3 below).

In accordance to the standard non-isothermal DSC results, where the un-infiltrated PEO block crystallized at higher temperatures than neat PEO (see Table 2), Fig. 14 shows that also isothermally the PEO block needs a lower undercooling for crystallization. Once again, the differences in polydispersity and synthesis procedures can account for such behavior, since the average chain length values are comparable.

Table 3
Avrami fitting parameters for the studied samples.

Sample	T_c (°C)	n	k (min^{-n})	$\tau^{1/2}{}_{theo}$ (min)	$\tau^{1/2}{}_{exp}$ (min)	R^2	Range (%)
EO_{100}^{100}	50.5	2.1	1.1E-01	2.4	2.4	1.0000	3–20
	51.0	2.1	6.5E-02	3.0	3.3	0.9999	3–20
	51.5	2.2	2.7E-02	4.5	4.8	0.9999	3–20
	52.0	2.0	1.0E-02	8.3	8.1	0.9993	3–20
	52.5	2.0	5.0E-03	11.1	11.0	0.9998	3–20
	53.0	2.0	2.0E-03	17.7	16.8	0.9998	3–20
	53.5	2.2	1.0E-03	21.2	21.4	0.9999	3–20
	54.0	2.1	1.0E-03	30.1	26.9	0.9990	3–20
EO_{100}^{100}/AAO 60 nm	−4.0	1.1	4.7E-01	1.4	1.4	0.9862	10–35
	−3.0	1.4	1.2E+00	0.7	0.7	0.9994	15–40
	−2.0	0.7	7.9E-01	0.8	0.7	0.9585	10–35
	−1.0	1.4	1.6E+00	0.6	0.6	0.9998	10–40
	0.0	0.9	1.4E+00	0.5	0.5	1.0000	15–40
	1.0	1.2	1.1E+00	0.7	0.7	0.9920	15–40
EO_{100}^{100}/AAO 35 nm	−8.0	1.3	1.3E-02	23.2	17.9	0.9665	3–30
Bd_{21}-*b*-EO_{79}^{257}	58.0	3.8	7.2E-05	11.2	11.9	0.9996	3–20
	57.0	3.4	4.4E-03	4.5	4.7	0.9998	3–20
	56.0	2.8	8.7E-02	2.1	2.3	0.9999	3–20
	55.0	2.8	5.8E-01	1.1	1.2	0.9996	3–20
	54.0	2.5	2.5E+00	0.6	0.7	0.9996	3–20
Bd_{21}-*b*-EO_{79}^{257}/ AA0 35 nm	−4.0	0.6	3.0E-01	4.5	4.9	0.9811	10–30
	−5.0	0.5	3.7E-01	3.7	5.9	0.9664	10–30
	−6.0	0.8	4.6E-01	2.9	1.7	0.9786	10–30
	−6.5	0.8	7.4E-01	1.9	1.0	0.9628	10–35
	−7.0	1.0	7.3E-01	1.9	1.0	0.9810	10–35
	−7.5	0.9	7.2E-01	2.9	1.0	0.9911	10–35

The overall isothermal crystallization kinetics data obtained by DSC was analyzed by the Avrami equation, closely following the procedure developed by Lorenzo et al. [146]. The Avrami equation [186] can be expressed as [146]:

$$1 - V_c(t - t_0) = \exp(-k(t - t_0)^n) \quad (2)$$

where V_c is the relative volumetric transformed fraction, t is the time variable, t_0 is the induction time or the time to start the detection of crystallization, k is the overall crystallization rate constant and n is the Avrami index. Table 3 reports the values of the fitting parameters: The Avrami index (n), the overall crystallization rate constant (k), the linear correlation coefficient (R^2), the conversion range employed for the fitting, the predicted ($\tau^{1/2}{}_{theo}$) and the experimentally determined ($\tau^{1/2}{}_{exp}$) half-crystallization times [146]. The conversion range employed for the fitting varied depending on whether the kinetics was determined by the usual continuous isothermal method (for un-infiltrated materials) or the step isothermal method (for infiltrated materials), see experimental. The values of k displayed trends that are similar to those of the half-crystallization times, once their dependence with the Avrami index is taken into account (i.e., if the values of k are elevated to the power $1/n$, then they can be expressed as min^{-1} and are easily compared with one another).

Up to 50% conversion to the crystalline state (i.e., during the entire primary crystallization), the Avrami equation can predict very well the overall crystallization process, since half crystallization times predicted by the Avrami fit are in general agreement with the experimental values, as reported in Table 3.

Müller et al. [147] have considered that the Avrami exponent is given by the addition of two terms:

$$n = n_n + n_{gd} \quad (3)$$

where n_n is the part of the exponent related to nucleation and n_{gd} that related to growth dimensionality. The n_n term can have values ranging from 0 to 1 by considering that nucleation can be instantaneous or sporadic. Fractional values may indicate that the nucleation is not purely instantaneous or purely sporadic, but that it follows a certain characteristic kinetics in between these two extremes; in fact, nucleation usually turns more sporadic as T_c increases.

The Avrami index values for the neat polydisperse PEO were found to be in the range 2.0–2.2 which is low as compared with the values that we have obtained in the past with closely monodisperse PEO samples (yielding Avrami index values in the expected range of 3–4 corresponding to spherulitic superstructures). Homopolymers that exhibit Avrami indexes close to 2 may crystallize in two dimensional arrays of lamellae (i.e., axialites) that normally impinge with one another (with a high nucleation density) before they can develop the three dimensional superstructure of spherulites. Then the Avrami index would correspond in this case to instantaneously nucleated axialites (i.e., $n_n = 0$ and $n_{gd} = 2$). In any case, for bulk homopolymers, the Avrami exponent ranges between 2 and 4, or in other words, the overall crystallization kinetics is characterized by orders always equal or greater than 2.

More reasonable values of the Avrami index were obtained for the PEO block within Bd_{21}-*b*-EO_{79}. The PEO block in this case constitutes the percolated matrix of this diblock copolymer that contains PB cylinders. The Avrami index values obtained increases from 2.5 at the lowest crystallization temperature to 3.8 for the maximum displaying an increasing trend with temperature. The results correspond to instantaneously nucleated spherulites (if we approximate the value to $n = 3$) that upon increasing

temperature become increasingly more sporadic (and the limit would be $n = 4$) as expected.

In the case of all the infiltrated materials examined here, a dramatic drop in the Avrami index was obtained. The range of values obtained for the infiltrated materials are all between 0.5 and 1.4 and a total of 12 different experiments (each one repeated 3 times) performed separately with different infiltrated materials and at different isothermal crystallization temperatures were performed, as reported in Table 3. This is the first time, as far as the authors are aware that first order (or close to first order, $n = 1$) overall crystallization kinetics are reported for polymeric nanocylinders infiltrated in AAO nanopores whose nucleation is homogeneous. When PEO and the PEO block of the Bd_{21}-b-EO_{79}^{257} diblock copolymer are confined into the AAO nanopores, they crystallize at extreme supercoolings, and their nucleation is most probably homogeneous. Under these circumstances, the rate determining step of the overall crystallization kinetics is the nucleation, since once a nucleus is produced inside one nanopore, crystal growth is extremely fast (see Fig. 14). So, this would be equivalent to consider that $n_{gd} = 0$ and the Avrami equation would be determined by just the nucleation rate. Then when the nucleation is sporadic we would expect a first order kinetics with $n = 1$.

First order kinetics have also been reported in the past for the crystallization of PEO spheres by Chen et al. [88], Massa and Kalnoki-Veress [29] and Reiter et al. [143].

Shin et al. and Woo et al. [157,163] studied the infiltration of a linear PE into AOO templates. They have reported values of the Avrami index that are close to 2 (between 1.7 and 1.9), which does not correspond to the expected first order kinetics for truly isolated and confined heterogeneity free MDs. Additionally, the crystallization temperature range employed is too high for homogeneous nucleation (T_c values greater than 70 °C). Given that the T_g values for polyethylene are around −30 or −120° C [187,188], the difference between T_c and T_g is of at least 100 °C. A surface nucleation mechanism is more plausible in this case. Polymers like PEO or PCL have been reported to nucleate homogeneously (also in the present work) at temperatures that are much closer to their corresponding T_g values, although the exact temperature depends on the MDs crystallizing volume [1,13,37].

Duran et al. [156] reported results on the infiltration of PP into alumina templates. The authors present results with several pore diameters. For larger pores they observed the phenomenon of fractionated crystallization but as they reduce the pore diameter, their results indicate that they have obtained exclusive confined crystallization of heterogeneity free MDs, since the PP peak crystallization values upon cooling from the melt are between 30 and 40 °C. These values could well be associated with PP homogeneous or surface nucleation. Nevertheless, they obtained Avrami index values that are much higher than 1, in fact most reported values are between 2 and 2.5. It is difficult to understand these results but they do not conform to the expectation for homogeneous or surface nucleation.

In the present work, we found that trying to perform conventional isothermal measurements with DSC on infiltrated templates was a challenge because the amount of polymer sample within the pores is very small with respect to the total sample weight (between 1 and 2%), as a result, the data was very noisy and unreliable. This is why we employ the step crystallization technique instead. We speculate that the use of conventional determinations of the isothermal crystallization kinetics by the continuous method may have been the reason why, in the previous works commented above [156,157,163], the expected first order kinetics, characteristic of confined and isolated heterogeneity free MDs, was not found.

Finally, Maiz et al. [170] studied the crystallization of confined PEO nanotubes inside AAO templates. They showed that when the size of the alumina nanopores is larger than a critical value, the infiltrated PEO does not form cylinders inside the nanopores anymore, but hollow cylinders or nanotubes. They performed limited isothermal crystallization experiments, but their T_c temperatures were too high for homogeneous nucleation to develop. The nanotubes probably started their crystallization from surface nuclei, however, the results indicate that the hollow nanotube ensemble was apparently confined and heterogeneity free, since a crystallization kinetics that approximated first order was reported.

7. Conclusions

Crystallization under confinement is present in many systems such as droplets, blends, block copolymers and nanopores within inorganic templates. As the degree of confinement increases, the predominance of heterogeneous nucleation decreases. When the number of heterogeneities is of the same order of magnitude than the number of MDs into which the polymer is divided, fractionated crystallization arises. If the number of MDs is several orders of magnitude higher than the number of existing active heterogeneities, heterogeneous nucleation can completely disappear (i.e., it becomes statistically insignificant). In this case, the ensemble of highly confined isolated MDs can undergo at increasing supercoolings: edge, surface or eventually homogenous nucleation. The practical consequences of confinement are: a very large decrease of the solidification temperature, a decrease of the degree of crystallinity and a moderate decrease in melting point.

Since macromolecules inside heterogeneity free MDs need very large supercoolings to nucleate, once a nucleation site is generated (e.g., by surface or homogeneous nucleation), its secondary nucleation or growth is usually instantaneous. The overall crystallization kinetics becomes dominated by the nucleation rate and becomes a simple first order process.

Surface nucleation requires lower supercoolings than classic volume homogeneous nucleation, because it is a process characterized by a lower free energy than the more energetically costly process of creating new crystal surfaces inside an MD volume. Therefore, in many cases where confinement has been induced and an isolated ensemble of heterogeneity free MDs has been produced, the nucleation starts at the surface or interface of the MDs.

The distinction between surface and homogeneous nucleation is not easy and many reports in the literature claim that they have found homogeneous nucleation simply because upon confinement the polymer crystallizes at large supercoolings.

In fact, homogeneous nucleation can only occur at extreme supercoolings and its characteristic crystallization temperature depends on the volume of the MDs. In the limit of a few nanometers (15–25 nm), homogeneous nucleation has been documented for polymers like PCL or PEO at temperatures which are only 5–15 °C above their glass transition temperatures. For polyethylene, we believe that homogeneous nucleation has never been achieved so far, since it crystallizes at much shallower undercoolings by surface nucleation. The reason for this particular phenomenon in PE is still unknown.

In order to demonstrate the existence of homogeneous nucleation for a confined polymeric sample (assuming that an ensemble of isolated and heterogeneity free MDs has been successfully prepared), at least two conditions should be fulfilled: (a) The crystallization must occur at the maximum possible supercooling (that depends on the volume of the MDs). This means that T_c should be as close to T_g as possible if the MD volume approaches very small values (typically 10–20 nm). (b) The isothermal overall crystallization kinetics must approach a first order or lower ($n \leq 1$), since the kinetics will be dominated by the nucleation process. Such first order crystallization kinetics can also be found for confined

polymers undergoing surface nucleation. We presented in this paper, for the first time, data that fulfills both previous conditions for the cases of PEO and the PEO block of the Bd_{21}-*b*-EO_{79}^{257} diblock copolymer when confined into AAO nanopores.

Acknowledgments

We are indebted to Prof. Nikos Hadjichristidis and Dr. George Sakellariou for generously providing the PB-*b*-PEO diblock copolymer employed for AAO infiltration studies.

References

[1] Wunderlich B. Macromolecular physics. In Crystal structure, morphology and defects, vol. 1. New York: Academic Press; 1973.
[2] Wunderlich B. Macromolecular physics. In Crystal nucleation, growth, annealing, vol. 2. New York: Academic Press; 1976.
[3] Wunderlich B. Macromolecular physics. In Crystal melting, vol. 3. New York: Academic Press; 1980.
[4] Mandelkern L. Crystallization of polymers. In Equilibrium concepts. 2nd ed., vol. 1. Cambridge: Cambridge University Press; 2002.
[5] Mandelkern L. Crystallization of polymers. In Kinetics and mechanisms. 2nd ed., vol. 2. Cambridge: Cambridge University Press; 2004.
[6] Schultz J. Polymer crystallization: the development of crystalline order in thermoplastic polymers. New York: Oxford University Press and American Chemical Society; 2001.
[7] Strobl GR. The physics of polymers: concepts for understanding their structures and behavior. 3rd ed. Berlin: Springer; 2007.
[8] Reiter G, Strobl GR, editors. Lecture notes in physics: progress in understanding of polymer crystallization, vol. 714. Berlin: Springer-Verlag; 2007.
[9] Piorkowska E, Rutledge GC, editors. Handbook of polymer crystallization. New Jersey: Wiley; 2013.
[10] Frensch H, Harnischfeger P, Jungnickel BJ. Fractionated crystallization in incompatible polymer blends. In: Utracky LA, Weiss RA, editors. Multiphase polymers: blends and ionomers ACS Symposium Series 395. Washington: American Chemical Society; 1989. p. 101–25.
[11] Müller AJ, Balsamo V, Arnal ML. Nucleation and crystallization in diblock and triblock copolymers. Adv Polym Sci 2005;190:1–63.
[12] Hamley IW. Crystallization in block copolymers. Adv Polym Sci 1999;148:113–37.
[13] Loo Y, Register A. Crystallization within block copolymer Mesophases. In: Hamley IW, editor. Developments in block copolymer science and technology. New York: Wiley; 2004.
[14] Castillo RV, Müller AJ. Crystallization and morphology of biodegradable or biostable single and double crystalline block copolymers. Prog Polym Sci 2009;34:519–60.
[15] Müller AJ, Balsamo V, Arnal ML. Crystallization in block copolymers with more than one crystallizable block. In: Reiter G, Strobl G, editors. Lecture notes in physics: progress in understanding of polymer crystallization, vol. 714. Berlin: Springer; 2007. p. 229–59.
[16] Müller AJ, Arnal M, Lorenzo AT. Crystallization in nano-confined polymeric systems. In: Piorkowska E, Rutledge G, editors. Handbook of polymer crystallization. New York: Wiley; 2013.
[17] Nadan B, Hsy J, Chen H. Crystallization behavior of crystalline-amorphous diblock copolymers consisting of a rubbery amorphous block. Polym Rev 2006;46(2):143–72.
[18] Van Riemsdyk A. Ann Chim Phys 1880;20(5):66.
[19] Price F. Nucleation in polymer crystallization. In: Zettlemoyer A, editor. Nucleation. New York: Marcel Dekker; 1969.
[20] Vonnegut B. Variation with temperature of the nucleation rate of supercooled liquid tin and water drops. J Colloid Sci 1948;3(6):563–9.
[21] Turnbull D, Cech R. Microscopic observation of the solidification of small metal droplets. J Appl Phys 1950;21(8):804–10.
[22] Pound G, La Mer V. Kinetics of crystalline nucleus formation in supercooled liquid tin. J Am Chem Soc 1952;74(9):2323–32.
[23] Turnbull D. Kinetics of solidification of supercooled liquid mercury droplets. J Chem Phys 1952;20(3):411–24.
[24] Turnbull D, Cormia R. Kinetics of crystal nucleation in some normal alkane liquids. J Chem Phys 1961;34(3):820–31.
[25] Cormia R, Price F, Turnbull D. Kinetics of crystal nucleation in polyethylene. J Chem Phys 1962;37(6):1333–40.
[26] Burns J, Turnbull D. Kinetics of crystal nucleation in molten isotactic polypropylene. J Appl Phys 1966;37(11):4021–6.
[27] Koutsky J, Walton A, Baer E. Nucleation of polymer droplets. J Appl Phys 1967;38(4):1832–9.
[28] Gornick F, Ross G, Frolen L. Crystal nucleation in polyethylene: the droplet experiment. J Polym Sci Pol Sym 1967;18(1):79–91.
[29] Massa MV, Dalnoki-Veress K. Homogeneous crystallization of Poly(Ethylene oxide) confined to droplets: the dependence of the crystal nucleation rate on length scale and temperature. Phys Rev Lett 2004;92(25):255509.
[30] Massa MV, Lee MSM, Dalnoki-Veress K. Crystal nucleation of polymers confined to droplets: Memory effects. J Polym Sci Part B Polym Phys 2005;43(23):3438–43.
[31] Massa MV, Carvalho JL, Dalnoki-Veress K. Confinement effects in polymer crystal nucleation from the bulk to few-chain systems. Phys Rev Lett 2006;97(24):247802.
[32] Carvalho JL, Massa MV, Dalnoki-Veress K. Ellipsometry as a probe of crystallization kinetics in thin diblock copolymer films. J Polym Sci Part B Polym Phys 2006;44(24):3448–52.
[33] Carvalho JL, Dalnoki-Veress K. Homogeneous bulk, surface, and edge nucleation in crystalline nanodroplets. Phys Rev Lett 2010;105:237801.
[34] Carvalho JL, Dalnoki-Veress K. Surface nucleation in the crystallisation of polyethylene droplets. Eur Phys J E 2011;34(6):1–6.
[35] Massa MV, Carvalho JL, Dalnoki-Veress K. Direct visualisation of homogeneous and heterogeneous crystallisation in an ensemble of confined domains of poly(ethylene oxide). Eur Phys J 2003;12(1):111–7.
[36] Arnal ML, Matos ME, Morales RA, Santana OO, Müller AJ. Evaluation of the fractionated crystallization of dispersed polyolefins in a polystyrene matrix. Macromol Chem Phys 1998;199(10):2275–88.
[37] Michell RM, Lorenzo AT, Müller AJ, Lin MC, Blaszczyk-Lezak I, Martín J, et al. The crystallization of confined polymers and block copolymers infiltrated within alumina nanotube templates. Macromolecules 2012;45(3):1517–28.
[38] Kailas L, Vasilev C, Audinot J, Migeon H, Hobbs J. A real-time study of homogeneous nucleation, growth, and phase transformations in nanodroplets of low molecular weight isotactic polypropylene using AFM. Macromolecules 2007;40(20):7223–30.
[39] Montenegro R, Landfester K. Metastable and stable morphologies during crystallization of alkanes in miniemulsion droplets. Langmuir 2003;19(15):5996–6003.
[40] Tongcher O, Sigel R, Landfester K. Liquid crystal nanoparticles prepared as miniemulsions. Langmuir 2006;22(10):4504–11.
[41] Taden A, Landfester K. Crystallization of poly(ethylene oxide) confined in miniemulsion droplets. Macromolecules 2003;36(11):4037–41.
[42] Ibarretxe Uriguen J, Bremer L, Mathot V, Groeninckx G. Preparation of waterborne dispersions of polyolefins: new systems for the study of homogeneous nucleation of polymers. Polymer 2004;45(17):5961–8.
[43] Ibarretxe Uriguen J, Bremer L, Mathot V, Groeninckx G. Preparation of waterborne dispersions of polyolefins: new systems for the study of homogeneous nucleation of polymers. Polymer 2004;45(17):5961–8.
[44] Weber C, Chiche A, Krausch G, Rosenfeldt S, Ballauf M, Harnau L, et al. Single lamella nanoparticles of polyethylene. Nano Lett 2007;7(7):2024–9.
[45] Jin Y, Rogunova M, Hiltner A, Baer E, Nowacki R, Galeski A, et al. Structure of polypropylene crystallized in confined nanolayers. J Polym Sci Part B Polym Phys 2004;42(18):3380–96.
[46] Bernal-Lara T, Liu R, Hiltner A, Baer E. Structure and thermal stability of polyethylene nanolayers. Polymer 2005;46(9):3043–55.
[47] Jin Y, Hiltner A, Baer E, Masirek R, Piorkowska E, Galeski A. Formation and transformation of smectic polypropylene nanodroplets. J Polym Sci Part B Polym Phys 2006;44(13):1795–803.
[48] Jin Y, Hiltnet A, Baer E. Fractionated crystallization of polypropylene droplets produced by nanolayer breakup. J Polym Sci Part B Polym Phys 2007;45(10):1138–51.
[49] Jin Y, Hiltner A, Baer E. Effect of a sorbitol nucleating agent on fractionated crystallization of polypropylene droplets. J Polym Sci Part B Polym Phys 2007;45(14):1788–97.
[50] Jin Y, Hiltner A, Baer E. Effect of an organic dicarboxylic acid salt on fractionated crystallization of polypropylene droplets. J Appl Polym Sci 2007;105(6):3260–73.
[51] Bernal-Lara T, Masirek R, Hiltner A, Baer E, Piorkowska E, Galeski A. Morphology studies of multilayered HDPE/PS systems. J Appl Polym Sci 2006;99(2):597–612.
[52] Puente Orench I, Stribeck N, Ania F, Baer E, Hiltner A, Baltá Calleja F. SAXS study on the crystallization of PET under physical confinement in PET/PC multilayered films. Polymer 2009;50(12):2680–7.
[53] Wang H, Keum J, Hiltner A, Baer E, Freeman B, Rozanski A, et al. Confined crystallization of polyethylene oxide in nanolayer assemblies. Science 2009;323(5915):757–60.
[54] Pethe V, Wang H, Hiltner A, Baer E, Freeman B. Oxygen and carbon dioxide permeability of EAA/PEO blends and microlayers. J Appl Polym Sci 2008;110(3):1411–9.
[55] Ma Y, Hu W, Reiter G. Lamellar crystal orientations biased by crystallization kinetics in polymer thin films. Macromolecules 2006;39(15):5159–64.
[56] Padden FJ, Keith HD. Crystallization in thin films of isotactic polypropylene. J Appl Phys 1966;37:4013–21.
[57] Cho K, Kim D, Yoon S. Effect of substrate surface energy on transcrystalline growth and its effect on interfacial adhesion of semicrystalline polymers. Macromolecules 2003;36(20):7652–60.
[58] Muratoglu OK, Argon AS, Cohen RE. Crystalline morphology of polyamide-6 near planar surfaces. Polymer 1995;36(11):2143–52.
[59] Pearce R, Vancso GJ. Imaging of melting and crystallization of poly(ethylene oxide) in real-time by hot-stage atomic force microscopy. Macromolecules 1997;30(19):5843–8.
[60] Tsuji M, Novillo LFA, Fujita M, Murakami S, Kohjiya S. Morphology of melt-crystallized poly(ethylene 2,6-naphthalate) thin films studied by transmission electron microscopy. J Mater Res 1999;14(1):251–8.

[61] Durell M, Macdonald JE, Trolley D, Wehrum A, Jukes PC, Jones RAL, et al. The role of surface-induced ordering in the crystallisation of PET films. Europhys Lett 2002;58:844–50.
[62] Basire C, Ivanov DA. Evolution of the lamellar structure during crystallization of a semicrystalline-amorphous polymer blend: time-resolved hot-stage SPM study. Phys Rev Lett 2000;85(26):5587–90.
[63] Lovinger AJ, Keith HD. Electron diffraction investigation of a high-temperature form of poly(vinylidene fluoride). Macromolecules 1979;12(5):919–24.
[64] Kovacs AJ, Straupe C. Isothermal growth, thickening and melting of poly(-ethylene oxide) single crystals in the bulk. Part 4. Dependence of pathological crystal habits on temperature and thermal history. Faraday Discuss 1979;68(0):225–38.
[65] Schonherr H, Frank CW. Ultrathin films of poly(ethylene oxides) on oxidized silicon. 1. Spectroscopic characterization of film structure and crystallization kinetics. Macromolecules 2003;36(4):1188–98.
[66] Abe H, Kikkawa Y, Iwata T, Aoki H, Akehata T, Doi Y. Microscopic visualization on crystalline morphologies of thin films for poly[(R)-3-hydroxybutyric acid] and its copolymer. Polymer 2000;41(3):867–74.
[67] Reiter G, Sommer J. Crystallization of adsorbed polymer monolayers. Phys Rev Lett 1998;80(17):3771–4.
[68] Reiter G, Sommer J. Polymer crystallization in quasi-two dimensions. I. Experimental results. J Chem Phys 2000;112(9):4376–84.
[69] Sommer J, Reiter G. Polymer crystallization in quasi-two dimensions. Ii. Kinetic models and computer simulations. J Chem Phys 2000;112(9):4384–94.
[70] Zhang F, Liu J, Huang H, Du B, He T. Branched crystal morphology of linear polyethylene crystallized in a two-dimensional diffusion-controlled growth field. Eur Phys J E 2002;8(3):289–97.
[71] Sakai Y, Imai M, Kaji K, Tsuji M. Tip-splitting crystal growth observed in crystallization from thin films of poly(ethylene terephthalate). J Cryst Growth 1999;203(1–2):244–54.
[72] Paul DR, Bucknall C, editors. Polymer blends, formulation and performance, vol. 1 and 2. New York: John Wiley and Sons; 2000.
[73] Santana O, Müller A. Homogeneous nucleation of the dispersed crystallisable component of immiscible polymer blends. Polym Bull 1994;32(4):471–7.
[74] Morales RA, Arnal ML, Müller AJ. The evaluation of the state of dispersion in immiscible blends where the minor phase exhibits fractionated crystallization. Polym Bull 1995;35(3):379–86.
[75] Manaure AC, Morales RA, Sánchez JJ, Müller AJ. Rheological and calorimetric evidences of the fractionated crystallization of iPP dispersed in ethylene/α-olefin copolymers. J App Polym Sci 1997;66(13):2481–93.
[76] Arnal ML, Müller AJ, Maiti P, Hikosaka M. Nucleation and crystallization of isotactic poly(propylene) droplets in an immiscible polystyrene matrix. Macromol Chem Phys 2000;201(17):2493–504.
[77] Tol R, Mathot V, Groeninckx G. Confined crystallization phenomena in immiscible polymer blends with dispersed micro-and nanometer sized PA6 droplets Part 4: polymorphous structure and (meta)-stability of PA6 crystals formed in different temperature regions. Polymer 2005;46(9):2966–77.
[78] Tol R, Mathot V, Groeninckx G. Confined crystallization phenomena in immiscible polymer blends with dispersed micro- and nanometer sized PA6 droplets, Part 3: crystallization kinetics and crystallinity of micro- and nanometer sized PA6 droplets crystallizing at high supercoolings. Polymer 2005;46(9):2955–65.
[79] Yordanov C, Minkova L. Fractionated crystallization of compatibilized LDPE/PA6 blends. Eur Polym J 2005;41(3):527–34.
[80] Fillon B, Wittman JC, Lotz B, Thierry A. Self-nucleation and recrystallization of isotactic polypropylene (α phase) investigated by differential scanning calorimetry. J Polym Sci Part B Polym Phys 1993;31(10):1383–93.
[81] Müller AJ, Arnal ML. Thermal fractionation of polymers. Prog Polym Sci 2005;30(5):559–603.
[82] Tol R, Mathot V, Groeninckx G. Confined crystallization phenomena in immiscible polymer blends with dispersed micro – and nanometer sized PA6 droplets, part 1: uncompatibilized PS/PA6, (PPE/PS)/PA6 and PPE/PA6 blends. Polymer 2005;46(2):369–82.
[83] Tol R, Mathot V, Groeninckx G. Confined crystallization phenomena in immiscible polymer blends with dispersed micro- and nanometer sized PA6 droplets, Part 2: reactively compatibilized PS/PA6 and (PPE/PS)/PA6 blends. Polymer 2005;46(2):383–96.
[84] Arnal ML, Müller AJ. Fractionated crystallisation of polyethylene and ethylene/α-olefin copolymers dispersed in immiscible polystyrene matrices. Macrom Chem Phys 1999;200(11):2559–76.
[85] Manaure A, Müller AJ. Nucleation and crystallization of blends of poly(-propylene) and ethylene/α-olefin copolymers. Macrom Chem Phys 2000;201(9):958–72.
[86] He Y, Weihua Z, Inoue Y. Nanoscale-confined and fractional crystallization of poly(ethylene oxide) in the interlamellar region of poly(butylene succinate). Macromolecules 2004;37(9):3337–45.
[87] Córdova ME, Lorenzo AT, Müller AJ, Gani L, Tencé-Girault S, Leibler L. The influence of blend morphology (co-continuous or sub-micrometer droplets dispersions) on the nucleation and crystallization kinetics of double crystalline polyethylene/polyamide blends prepared by reactive extrusion. Macromol Chem Phys 2011;212(13):1335–50.
[88] Chen HL, Wu JC, Lin TL, Lin JS. Crystallization kinetics in microphase-separated poly(ethylene oxide)-block-poly(1,4-butadiene). Macromolecules 2001;34(20):6936–44.
[89] Boschetti-de-Fierro A, Lorenzo AT, Müller AJ, Schmalz H, Abetz V. Crystallization kinetics of PEO and PE in different triblock terpolymers: effect of microdomain geometry and confinement. Macromol Chem Physic 2008;209(5):476–87.
[90] Loo YL, Register RA, Ryan AJ. Polymer crystallization in 25-nm spheres. Phys Rev Lett 2000;84(18):4120–3.
[91] Abetz V. Block copolymers. In: Encyclopedia of polymer science and engineering. New York: John Wiley & Sons; 2001.
[92] Abetz V. Assemblies in complex block copolymer systems. In: Supramolecular polymers. New York: Marcel Dekker Inc; 2000.
[93] Hamley I. The physics of block copolymers. London: Oxford University Press; 1998.
[94] Müller AJ, Arnal ML, Trujillo M, Lorenzo AT. Super-nucleation in nanocomposites and confinement effects on the crystallizable components within block copolymers, Miktoarm star copolymers and nanocomposites. Eur Polym J 2011;47(4):614–29.
[95] Nojima S, Ohguma Y, Namiki S, Ishizone T, Yamaguchi K. Crystallization of homopolymers confined in spherical or cylindrical nanodomains. Macromolecules 2008;41(6):1915–8.
[96] Castillo RV, Arnal ML, Müller AJ, Hamley IW, Castelletto V, Schmalz H, et al. Fractionated crystallization and fractionated melting of confined PEO microdomains in PB-b-PEO and PE-b-PEO diblock copolymers. Macromolecules 2008;41(3):879–89.
[97] Röttele A, Thurn-Albrecht T, Sommer JU, Reiter G. Thermodynamics of formation, reorganization, and melting of confined nanometer-sized polymer crystals. Macromolecules 2003;36(4):1257–60.
[98] Huang YY, Chen HL, Li HC, Lin TL, Lin JS. Coalescence of crystalline microdomains driven by postannealing in a block copolymer blend. Macromolecules 2003;36(2):282–5.
[99] Huang Y, Yang C, Chen H, Chiu F, Lin T, Liou W. Crystallization-induced microdomain coalescence in sphere-forming crystalline–amorphous diblock copolymer systems: neat diblock versus the corresponding blends. Macromolecules 2004;37(2):486–93.
[100] Müller AJ, Balsamo V, Arnal ML, Jakob T, Schmalz H, Abetz V. Homogeneous nucleation and fractionated crystallization in block copolymers. Macromolecules 2002;35(8):3048–58.
[101] Molinuevo CH, Mendez GA, Müller AJ. Nucleation and crystallization of PET droplets dispersed in an amorphous PC matrix. J Appl Polym Sci 1998;70(9):1725–35.
[102] Arnal ML, Balsamo V, López-Carrasquero F, Contreras J, Carrillo M, Schmalz H, et al. Synthesis and characterization of polystyrene-b-poly(ethylene oxide)-b-poly(ε-caprolactone) block copolymers. Macromolecules 2001;34(23):7973–82.
[103] Michell RM, Müller AJ, Deshayes G, Dubois P. Effect of sequence distribution on the isothermal crystallization kinetics and successive self-nucleation and annealing (SSA) behavior of poly(ε-caprolactone-co-ε-caprolactam) copolymers. Eur Polym J 2010;46(6):1334–44.
[104] Li Z, Liu R, Mai B, Wang W, Wu Q, Liang G, et al. Temperature-induced and crystallization-driven self-assembly of polyethylene-b-poly(ethylene oxide) in solution. Polymer 2013;54(6):1663–70.
[105] Yin L, Hillmyer M. Disklike Micelles in water from polyethylene-containing diblock copolymers. Macromolecules 2011;44(8):3021–8.
[106] Qi F, Guerin G, Cambridge G, Xu W, Manners I, Winnik M. Influence of solvent polarity on the self-assembly of the crystalline–coil diblock copolymer polyferrocenylsilane-b-polyisoprene. Macromolecules 2011;44(15):6136–44.
[107] Gilroy J, Gadt T, Whittell G, Chabanne L, Mitchels J, Richardson R. Monodisperse cylindrical micelles by crystallization-driven living self-assembly. Nat Chem 2010;2(7):566–70.
[108] Lazzari M, Lopez-Quintela M. Micellization Phenomena in semicrystalline block copolymers: reflexive and critical views on the formation of cylindrical micelles. Macromol Rapid Commun 2009;30(21):1785–91.
[109] Gao L, Zhang K, Chen YM. Functionalization of shaped polymeric nanoobjects via bulk co-self-assembling gelable block copolymers with silane coupling agents. Polymer 2011;52(17):3681–6.
[110] Shi Z, Lu H, Chen Z, Cheng R, Chen D. Rational design, syntheses, characterization and solution behavior of amphiphilic azobenzene-containing linear-dendritic block copolymers. Polymer 2012;53(2):359–69.
[111] She M, Ho R. Formation of conductive polyaniline nanoarrays from block copolymer template via electroplating. Polymer 2012;53(13):2628–32.
[112] Petzetakis N, Walker D, Dove A, O'Reilly R. Crystallization-driven sphere-to-rod transition of poly(lactide)-b-poly(acrylic acid) diblock copolymers: mechanism and kinetics. Soft Matter 2012;8(28):7408–14.
[113] Li Z, Ono R, Wu Z, Bielawski C. Synthesis and self-assembly of poly(hexylthiophene)-block-poly(acrylic acid). Chem Commun 2011;47(1):197–9.
[114] Qin S, Li H, Yuan W, Zhang Y. Hierarchical self-assembly of fluorine-containing diblock copolymer: from onion-like nanospheres to superstructured microspheres. Polymer 2011;52(4):1191–6.
[115] Bian Q, Xiao Y, Lang M. Thermoresponsive biotinylated star amphiphilic block copolymer: synthesis, self-assembly, and specific target recognition. Polymer 2012;53(8):1684–93.
[116] Xu L, Zhang X, Yang H, Li X, Li C, Zhang S. Vesicle formation of polystyrene-block-poly (ethylene oxide) block copolymers induced by supercritical CO_2 treatment. Polymer 2010;51(16):3808–13.

[117] Fu J, Luan B, Yu X, Cong Y, Li J, Pan C, et al. Self-assembly of crystalline–coil diblock copolymer in solvents with varying selectivity: from spinodal-like aggregates to spheres, cylinders, and lamellae. Macromolecules 2004;37(3):976–86.
[118] Chen Y, Zhang F, Xie X, Yuan J. Effects of micelle structures formed in selective solvents on crystallization behaviors of poly(ethylene glycol)-b-poly(styrene) copolymers. Polymer 2007;48(8):2755–61.
[119] Yu C, Chuang Y, Tung S. Self-assembly of polystyrene-b-poly(4-vinylpyridine) in deoxycholic acid melt. Polymer 2011;52(18):3994–4000.
[120] Yi F, Yu R, Zheng S, Li X. Nanostructured thermosets from epoxy and poly(2,2,2-trifluoroethyl acrylate)-block-poly(glycidyl methacrylate) diblock copolymer: demixing of reactive blocks and thermomechanical properties. Polymer 2011;52(24):5669–80.
[121] Mihut A, Chiche A, Drechsler M, Schmalz H, Di Cola E, Krausch G, et al. Crystallization-induced switching of the morphology of poly(ethylene oxide)-block-polybutadiene micelles. Soft Matter 2009;5(1):208–13.
[122] Mihut A, Drechsler M, Moller M, Ballauff M. Sphere-to-rod transition of micelles formed by the semicrystalline polybutadiene-block-poly(ethylene oxide) block copolymer in a selective solvent. Macromol Rapid Commun 2010;31(5):449–53.
[123] Du Z, Xu J, Fan Z. Regulation of micellar morphology of PCL-b-PEO block copolymers by crystallization temperature. Macromol Rapid Commun 2008;29(6):467–71.
[124] Zheng J, Xiong H, Chen W, Lee K, Horn R, Quirk R, et al. Onsets of tethered chain overcrowding and highly stretched brush regime via crystalline–amorphous diblock copolymers. Macromolecules 2006;39(2):641–50.
[125] Petzetakis N, Dove A, Reilly R. Cylindrical micelles from the living crystallization-driven self-assembly of poly(lactide)-containing block copolymers. Chem Sci 2011;2(5):955–60.
[126] Zhao Y, Shi X, Gao H, Zhang L, Zhu F, Wu Q. Thermo- and pH-sensitive polyethylene-based diblock and triblock copolymers: synthesis and self-assembly in aqueous solution. J Mater Chem 2012;22(12):5737–45.
[127] Schmalz H, Schmelz J, Drechsler M, Yuan J, Walther A, Schweimer K, et al. Thermo-reversible formation of wormlike micelles with a microphase-separated corona from a semicrystalline triblock terpolymer. Macromolecules 2008;41(9):3235–42.
[128] Schmelz J, Karg M, Hellweg T, Schmalz H. General pathway toward crystalline-core micelles with tunable morphology and corona segregation. ACS Nano 2012;5(12):9523–34.
[129] Massey J, Temple K, Cao L, Rharbi Y, Raez J, Winnik M, et al. Self-assembly of organometallic block copolymers: the role of crystallinity of the core-forming polyferrocene block in the micellar morphologies formed by poly(ferrocenylsilane-b-dimethylsiloxane) in n-alkane solvents. J Am Chem Soc 2000;122(47):11577–84.
[130] Raez J, Manners I, Winnik M. Fiberlike structures from the self-assembly of a highly asymmetric poly(ferrocenyldimethylsilane-b-dimethylsiloxane) in dilute solution. Langmuir 2002;18(19):7229–39.
[131] Guerin G, Raez J, Manners I, Winnik M. Light scattering study of rigid, rodlike organometallic block copolymer micelles in dilute solution. Macromolecules 2005;38(18):7819–27.
[132] Raez J, Manners I, Winnik M. Nanotubes from the self-assembly of asymmetric crystalline–coil poly(ferrocenylsilane–siloxane) block copolymers. J Am Chem Soc 2002;124(35):10381–95.
[133] Mihut AM, Crassous JJ, Schmalz H, Ballauff M. Crystallization-induced aggregation of block copolymer micelles: influence of crystallization kinetics on morphology. Colloid Polym Sci 2010;288(5):573–8.
[134] Mihut A, Crassous J, Schmalz H, Drechsler M, Ballauff M. Self-assembly of crystalline–coil diblock copolymers in solution: experimental phase map. Soft Matter 2012;8(11):3163–73.
[135] Wang X, Wang H, Frankowski D, Lam P, Welch P, Winnik M, et al. Growth and crystallization of metal-containing block copolymer nanotubes in a selective solvent. Adv Mater 2007;19(17):2279–85.
[136] Wang J, Horton J, Liu G, Lee S, Shea K. Polymethylene-block-poly(dimethyl siloxane)-block-polymethylene nanoaggregates in toluene at room temperature. Polymer 2007;48(14):4123–9.
[137] Lin E, Gast A. Semicrystalline diblock copolymer platelets in dilute solution. Macromolecules 1996;29(12):4432–41.
[138] Richter D, Schneiders D, Monkenbusch M, Willner L, Fetters L, Huang J, et al. Polymer aggregates with crystalline cores: the system polyethylene–poly(ethylenepropylene). Macromolecules 1997;30(4):1053–68.
[139] Ramzi A, Prager M, Richter D, Efstratiadis V, Hadjichristidis N, Young R, et al. Influence of polymer architecture on the formation of micelles of miktoarm star copolymers polyethylene/poly(ethylenepropylene) in the selective solvent decane. Macromolecules 1997;30(23):7171–82.
[140] Radulescu A, Mathers R, Coates G, Richter D, Fetters L. A SANS study of the self-assembly in solution of syndiotactic polypropylene homopolymers, syndiotactic polypropylene-block-poly(ethylene-co-propylene) diblock copolymers, and an alternating atactic–isotactic multisegment polypropylene. Macromolecules 2004;37(18):6962–71.
[141] Li Z, Liu R, Mai B, Feng S, Wu Q, Liang G, et al. Synthesis and self-assembly of isotactic polystyrene-block-poly(ethylene glycol). Polym Chem 2013;4(4):954–60.
[142] Rochette CN, Rosenfeldt S, Henzler K, Polzer F, Ballauff M, Tong Q, et al. Annealing of single lamella nanoparticles of polyethylene. Macromolecules 2011;44(12):4845–51.
[143] Reiter G, Castelein G, Somm JU, Röttele A, Thurn-Albrecht T. Direct visualization of random crystallization and melting in arrays of nanometer-size polymer crystals. Phys Rev Lett 2001;87(22):226101.
[144] Tol R, Minakov A, Adamovsky S, Mathot V, Schick C. Metastability of polymer crystallites formed at low temperature studied by ultra fast calorimetry: polyamide 6 confined in sub-micrometer droplets vs. bulk PA6. Polymer 2006;47(6):2172–8.
[145] Martín J, Maiz J, Sacristan J, Mijangos C. Tailored polymer-based nanorods and nanotubes by "template synthesis": from preparation to applications. Polymer 2012;53(6):1149–66.
[146] Lorenzo AT, Arnal ML, Albuerne J, Müller AJ. DSC isothermal polymer crystallization kinetics measurements and the use of the avrami equation to fit the data: guidelines to avoid common problems. Polym Test 2007;26(2):222–31.
[147] Balsamo V, Urdaneta N, Pérez L, Carrizales P, Abetz V, Müller AJ. Effect of the polyethylene confinement and topology on its crystallization within semicrystalline ABC triblock copolymers. Eur Polym J 2004;40(6):1033.
[148] Galante M, Mandelkern L, Alamo R, Lehtinen A, Paukkeri R. Crystallization kinetics of metallocene type polypropylenes. J Therm Anal 1996;47(4):913–29.
[149] Masuda H, Fukuda K. Ordered metal nanohole arrays made by a two-step replication of honeycomb structures of anodic alumina. Science 1995;268(5216):1466–8.
[150] Steinhart M. Supramolecular organization of polymeric materials in nanoporous hard templates. Adv Polym Sci 2008;220:123–87.
[151] Martin CR. Nanomaterials - a membrane-based synthetic approach. Science 1994;266(5193):1961–6.
[152] Martin CR. Template synthesis of electronically conductive polymer nanostructures. Acc Chem Res 1995;28(2):61–8.
[153] Martín J, Mijangos C. Tailored polymer-based nanofibers and nanotubes by means of different infiltration methods into alumina nanopores. Langmuir 2009;25(2):1181–7.
[154] Steinhart M, Wendorff J, Greiner A, Wherspohn R, Nielsch K, Schilling J, et al. Polymer nanotubes by wetting of ordered porous templates. Science 2002;296:1997.
[155] Zhang M, Dobriyal P, Chen J-T, Russell T, Olmo J, Merry A. Wetting transition in cylindrical alumina nanopores with polymer melts. Nano Lett 2006;6(5):1075–9.
[156] Duran H, Steinhart M, Hans-Jürgen B, Floudas G. From heterogeneous to homogeneous nucleation of isotactic Poly(propylene) confined to nanopotous alumina. Nano Lett 2011;11(4):1671–5.
[157] Shin K, Woo E, Jeong YG, Kim C, Huh J, Kim K-W. Crystalline structures, melting, and crystallization of linear polyethylene in cylindrical nanopores. Macromolecules 2007;40(18):6617–23.
[158] Garcia-Gutiérrez M-C, Linares A, Hernández JJ, Rueda DR, Ezquerra TA, Poza P, et al. Confinement-induced one-dimensional ferroelectric polymer arrays. Nano Lett 2010;10(4):1472–6.
[159] Hui W, Wei W, Huang Y, Wang C, Su Z. Polymorphic behavior of syndiotactic polystyrene crystallized in cylindrical nanopores. Macromolecules 2008;41(20):7755–8.
[160] Lutkenhaus JL, McEnnis K, Serghei A, Russell TP. Confinement effects on crystallization and curie transitions of poly(vinylidene fluoride-co-trifluoroethylene). Macromolecules 2010;43(8):3844–50.
[161] Steinhart M, Haissam PG, Prabhukaran M, Gösele U. Coherent kinetic control over crystal orientation in macroscopic ensembles of polymer nanorods an nanotubes. Phys Rev Lett 2006;97:027801.
[162] Steinhart M, Senz S, Wehrspohn RB, Gösele U, Wendorff JH. Curvature-directed crystallization of poly(vinylidene difluoride) in nanotube walls. Macromolecules 2003;36(10):3646–51.
[163] Woo E, Huh J, Jeong YG, Shin K. From homogeneous to heterogeneous nucleation of chain molecules under nanoscopic cylindrical confinement. Phys Res Lett 2007;98(13):136103.
[164] Wu H, Wang W, Huang Y, Su Z. Orientation of syndiotactic polystyrene crystallized in cylindrical nanopores. Macromol Rapid Commun 2009;30(3):194–8.
[165] Wu H, Wang W, Yang H, Su Z. Crystallization and orientation of syndiotactic polystyrene in nanorods. Macromolecules 2007;40(12):4244–9.
[166] Wu H, Su Z, Takahara A. Isotactic polystyrene nanorods with gradient crystallite states. Soft Matter 2012;8(11):3180–4.
[167] Suzuki Y, Duran H, Steinhart M, Butt HJ, Floudas G. Homogeneous crystallization and local dynamics of poly(ethylene oxide) (PEO) confined to nanoporous alumina. Soft Matter 2013;9(9):2621–8.
[168] Maiz J, Schäfer H, Rengarajan GT, Hartmann-Azanza B, Eickmeier H, Haase M, et al. How gold nanoparticles influence crystallization of polyethylene in rigid cylindrical nanopores. Macromolecules 2013;46(2):403–12.
[169] Shin K, Xiang H, Moon SI, Kim T, McCarthy TJ, Russell TP. Curving and frustrating Flatland. Science 2004;306:76.
[170] Maiz J, Martin J, Mijangos C. Confinement effects on the crystallization of poly(ethylene oxide) nanotubes. Langmuir 2012;28(33):12296–303.
[171] Quiram DJ, Register RA, Marchand GR. Crystallization of asymmetric diblock copolymers from microphase-separated melts. Macromolecules 1997;30(16):4551–8.
[172] Quiram DJ, Register RA, Marchand GR, Adamson DH. Chain orientation in block copolymers exhibiting cylindrically confined crystallization. Macromolecules 1998;31(15):4891–8.
[173] Huang P, Guo Y, Quirk RP, Ruan J, Lotz B, Thomas EL, et al. Comparison of poly(ethylene oxide) crystal orientations and crystallization behaviors in nano-confined cylinders constructed by a poly (ethylene oxide)-b-

polystyrene diblock copolymer and a blend of poly(ethylene oxide)-b-polystyrene and polystyrene. Polymer 2006;47(15):5457–66.
[174] Loo YL, Register RA, Adamson DH. Polyethylene crystal orientation induced by block copolymer cylinders. Macromolecules 2000;33(22):8361–6.
[175] Huang P, Zhu L, Cheng SZD, Ge Q, Quirk RP, Thomas EL, et al. Crystal orientation changes in two-dimensionally confined nanocylinders in a poly(ethylene oxide)-b-polystyrene/polystyrene blend. Macromolecules 2001;34(19):6649–57.
[176] Nojima S, Ohguma Y, Kadena K, Ishizone T, Iwasaki Y, Yamaguchi K. Crystal orientation of poly(ε-caprolactone) homopolymers confined in cylindrical nanodomains. Macromolecules 2010;43(8):3916–23.
[177] Guan Y, Liu G, Gao P, Li L, Ding G, Wang D. Manipulating crystal orientation of poly(ethylene oxide) by nanopores. ACS Macro Lett 2013;2(3):181–4.
[178] Xiong S, Wang Q, Xia H. Preparation of polyaniline nanotubes array based on anodic aluminum oxide template. Mater Res Bull 2004;39(10):1569–80.
[179] Lin MC, Nandan B, Chen HL. Mediating polymer crystal orientation using nanotemplates from block copolymer microdomains and anodic aluminium oxide nanochannels. Soft Matter 2012;8(28):7306–22.
[180] Wu H, Su Z, Takahara A. Characterization of an isotactic polystyrene/poly(2,6-dimethylphenylene oxide) nanorod blend with gradient composition and crystallinity. RSC Adv 2012;2(23):8707–12.
[181] Li M, Wu H, Huang Y, Su Z. Effects of temperature and template surface on crystallization of syndiotactic polystyrene in cylindrical nanopores. Macromolecules 2012;45(12):5196–200.
[182] Oh S, Kim Y, Choi Y-Y, Kim D, Choi H, No K. Fabrication of vertically well-aligned P(VDF-TrFE) nanorod arrays. Adv Mater 2012;24(42):5708–12.
[183] Xiang H, Shin K, Kim T, Moon SI, McCarthy TJ, Russell TP. From cylinders to helices upon confinement. Macromolecules 2005;38(4):1055–6.
[184] Dobriyal P, Xiang H, Kazuy M, Russell TP. Cylindrically confined diblock copolymers. Macromolecules 2009;42(22):9082–8.
[185] Sevink GJA, Zvelindovsky AV, Fraaije JGE, Huinink HP. Morphology of symmetric block copolymer in a cylindrical pore. J Chem Phys 2001;115(17):8226–30.
[186] Avrami M. Granulation, phase change and microstructure kinetics of phase change III. J Chem Phys 1941;9(2):177–84.
[187] McCrum N, Read B, Williams G. Anelastic and dielectric effects in polymeric solids. New York: Dover Publications Inc; 1967.
[188] Yamamoto K, Kato K, Sugino Y, Hara S, Miwa Y, Sakaguchi M, et al. Esr study on segmental motion of polyethylene in amorphous region, dependent on crystallinity, molecular weight, and labeled site. Macromolecules 2005;38(11):4737–43.

Rose Mary Michell (born 1981) is a Materials Engineer with an M.Sc. in materials engineering from Simón Bolívar University and she is about to finish her PhD at the same institution. She is a junior assistant professor at the Materials Science department of Simón Bolívar University. Rose Mary Michell's fields of interests include: nucleation, crystallization and morphology of semi-crystalline multiphasic polymers, copolymers and biopolymers.

Iwona Błaszczyk-Łężak received his PhD in Chemistry from the Centre of Molecular and Macromolecular Studies, Polish Academy of Sciences in Lodz in 2006. She specialized in the preparation of hard silicon-based thin-film materials and optically active thin films for sensor applications by remote plasma CVD. This subject studded deeply during her 2 years postdoctoral research stage at the Institute of Materials Science of Seville (CSIC-US). Her current research at the Institute of Polymer Science and Technology (CSIC) in Madrid focuses on the preparation of polymeric one-dimensional nanostructures by means of template-based techniques and on the study of dynamics of polymers under nanoconfinement.

Carmen Mijangos is, since 2000, Research Professor at the Polymers Science and Technology Institute of CSIC, Madrid, Spain. She received her doctoral degree in 1978 in Polymer Chemistry in the University of Basque Country. After some years in the University of Basque Country, Polytechnic University of Cataluña and CNRS (Lyon, France), she became scientific researcher of CSIC in 1984, in Madrid. In 2007, she started a new line of research on Fabrication and Characterization of 1D Polymer-based Nanostructures. The two other research lines are focused on Polymer Gelification and Modification. Their research interest goes from fundamental aspects of science to the development of novel materials. Among others, Prof. Mijangos is authored of near 200 SCI papers and books-chapters, 40 technical documents and patents. She is leader of the group nanostructured polymers and gels (www.nanopoly-gel.net). She has been director of the Institute of Polymers and Scientific Manager of Materials Area of CSIC. She has been nominated Academician of the Basque Academy of Science, Arts and Literature and she belongs to Ethics Committee of CSIC.

Prof. A.J. Müller is a Materials Engineer, with an M.Sc. in Chemistry and a Ph.D. in Physics (from Bristol University, U.K.). He leads the Simón Bolívar University polymer group and is a Full Professor in Materials Science. He has co-authored more than 200 publications. He has tutored 85 B.Sc. thesis and 48 postgraduate thesis (both M.Sc. and Ph.D.). He has won several awards in Venezuela, including the Lorenzo Mendoza Fleury, Polar Prize for basic science. In 2011 he received the international "Paul J. Flory Polymer Research Prize" (from Polychar). Prof. Müller has delivered more than 50 invited lectures at international conferences around the world. He has achieved an *h index* of 35. He is a corresponding member of the Venezuelan National Academy of Engineering and Habitat. His fields of interests include: polymer solution rheology, structured fluids, morphology, nucleation, crystallization and crystallization kinetics of semi-crystalline materials and of multiphasic materials (in particular polymer blends, block copolymers, biopolymers and nanocomposites). He is the president of the Venezuelan Polymer Association https://sites.google.com/a/usb.ve/ajmuller/.